Circumstellar Carbon Condensation: I. Low-p,T stabilities of Polyaromatic Hydrocarbons

A. Goeres, R. Keller, E. Sedlmayr, H.-P. Gail

Abstract To investigate the carbon condensation process in the cool envelopes of carbon-rich supergiant stars (C-stars), the stabilities of linear and polyaromatic hydrocarbons (PAHs) up to 26 carbon atoms have been calculated for an H/C-ratio of 2000, according to the particular elemental mixture in those objects. The study comprises closed shell species as well as radicals. The data is based on molecular mechanics calculations for most of the heats of formation and on group additivity rules for entropies and heat capacities. Based on an analysis of the particular physical situation in the condensation zone of C-star envelopes, in the range of $n_g = 10^{13}$ to $10^6\,\mathrm{cm}^{-3}$ for the gas particle density and temperatures from 1 200 to 500 K, the equilibrium situation of the gas, the chemical pathways to PAHs and the PAH formation rates are discussed.

1 Introduction

The polymerization of acetylene to a complex mixture of polyaromatic hydrocarbons is of considerable practical importance and, for this reason, has been a subject for extensive chemical research. For combustion of hydrocarbon fuels under terrestrial and laboratory conditions, a huge amount of detailed information has accumulated during the last decades concerning the reaction steps and their intermediates and a general picture has emerged of the dominating reaction mechanisms leading to the formation of large polyaromatic molecules.

The formation of soot from small hydrocarbons in the gas phase also is an ubiquitous process in space and seems to be responsible for the formation of more than one half of the observed interstellar condensed matter (the remaining fraction being mainly some kind of solid Fe-Mg-silicate). The source of the small interstellar carbon dust grains are the envelopes of carbon rich supergiant stars [1]. Since astrophysicists realized that outflows from such stars can be considered to be a special kind of sooting acetylene flame, the chemistry of carbon dust forming cool giant stars has been investigated by applying methods and results of laboratory combustion chemistry to this problem. This approach led to the prediction of the existence of polyaromatic hydrocarbons (PAHs) in space by Keller and Sedlmayr [2] one year before their existence was inferred by identifying some long known strong infrared emission features in carbon rich objects with vibrational features of PAHs by Léger and Puget [3]. Chemical rate networks have been developed for modeling the condensation of cosmic carbon dust particles by formation and growth of PAHs in stellar outflows by Keller [4], Frenklach and Feigelson [5], and Cherchneff et al. [6].

Nevertheless, the question whether cosmic carbon dust is formed via PAH formation remained open up to now. Though it seems to be quite clear that the cosmic carbon production occurs under conditions roughly similar to laboratory acetylene combustion, and in spite of the fact that all carbon rich cool supergiant stars *are observed* to be very efficient soot factories, the attempts to model a detailed PAH chemistry in circumstellar envelopes up to now failed in producing any significant amount of carbon dust from the gas phase.

The reason for this enigma seems to be related, in our opinion, to some fundamental and not yet properly accounted for differences between the conditions encountered in a stellar "acetylene flame" and in laboratory acetylene combustion. In all previous investigations, the thermodynamic conditions of the chemistry in flames seem to be incompletely transformed to the cosmic "flame":

- Carbon dust formation in space according to observations occurs at temperatures below 1 000 K (e.g. [7]). In contrast to terrestrial flames, where reactions of thermally activated closed shell species compete with free radical reactions, in stellar envelopes the latter ones predominate over reactions with activation barriers at such low temperatures.
- The densities in the condensation zone of cool giant stars are typically below 10^{-9} bar, which has strong implications for the reaction kinetics:
  - Three body collisions mostly are negligible at these extremely low pressures, and some key reaction rates have to be calculated in the low pressure limit [5].
  - The thermodynamic stability of the molecules is *not* mainly determined by their enthalpy, but it is strongly influenced by their entropy which favors highly unsaturated species [8].
  - The assumption of local thermodynamic equilibrium does not hold because effects of radiative energy transfer and radiative transitions in many cases exceed the effects of collisions [9].
- The envelope of a supergiant star with a circumstellar dust shell is a highly complex system where the thermodynamical conditions for the chemistry in the outflowing gas are sensitively controlled by the rate of dust formation. Only a *selfconsistent* treatment of the time-dependent chemistry, dust formation and growth, hydrodynamics and radiative transfer and of the mutual coupling of these processes guarantees reliable results with respect to the properties of carbon dust formed in a stellar environment and the yield of its production [10].

Especially the last requirement poses a serious computational problem, since a detailed chemical network for a huge number of hydrocarbon species has to be solved simultaneously with the equations regarding the physical conditions. In full generality, this huge and extremely stiff system of nonlinear differential-algebraic equations even exceeds the capacity of present supercomputers. Since the chemical equations necessarily has to be treated within the inner loop of the code, only a very fast chemical subroutine allows to overcome the computational difficulties, which contradicts the requirement for completeness.

Fortunately, the physics of the system under consideration allows the reduction of the chemical input for such numerical simulations to the knowledge of the *dominating reaction pathway* together with its kinetics, which leads to the required fast chemical code. This information can be obtained from an analysis of the chemical processes based on chemical thermodynamics considerations which additionally allow for the non–equilibrium effects mentioned above. In this paper we present the basic thermochemical data for the hydrocarbons involved in the carbon dust formation process and the results of the first part of an analysis of the reaction pathway. This will form the basis for a more detailed analysis of the reaction kinetics and for a thorough discussion of the physical conditions for carbon dust formation in the envelopes of carbon–rich giant stars, including the important non–equilibrium effects, in a subsequent paper [11], henceforth called paper II. Our complete analysis widely follows the scope and the methods of the paper of Stein and Fahr [12] on laboratory acetylene polymerization, but complementing it by:

- a completely different range of pressures and temperatures,
- including new group data for highly unsaturated radicals,
- a more detailed investigation of the reaction kinetics along the chemical pathway, and
- a discussion of the influence of some nonequilibrium effects on reaction kinetics at extremely low pressures.

The plan of the first part of the analysis in the present paper is as follows: Section 2 describes the general properties of circumstellar dust shells around cool supergiant stars, section 3 describes the methods used and the scope of this paper. Section 4 is the central part of this paper. It describes the molecular structure and presents the thermodynamical data for 149 hydrocarbons containing up to 26 carbon atoms, including new PAH–heats of formation and new radical group values. Section 5 gives a discussion of the concentrations of the various hydrocarbons as a function of temperature and pressure, based on the material of sect. 4. Section 6 finally presents the resulting zero-order pathways to carbon dust formation and the nucleation rates in stellar envelopes.

2 The Physical Situation in the condensation zone

The main interest of this paper is the investigation of the particular chemistry which controls the soot formation in the so called "C-stars". C-stars are a subclass of supergiant stars which are a late stage of the stellar evolution. A typical sun–like star after exhausting its hydrogen by nuclear burning transforms to a helium burning giant star. During this stage, most of the stars cool down to temperatures which allow for condensation processes close to the stellar photosphere. Since dust is a very efficient absorber, radiation pressure accelerates the dust, thus driving a massive outflow of dust and gas with a mass–loss rate of the order of 10^{-7} to 10^{-4} $M_\odot/yr$[1]. Depending on the inner processes of those stars, these extended envelopes of gas and dust show essentially two completely different types of chemistry: Stars with an approximately sun–like elemental composition with less carbon than oxygen (called M-stars) mainly produce silicates and Fe/Mg minerals, whereas the C-stars show an enhanced carbon (and sometimes nitrogen) abundance, which is the main product of the helium burning of the star. Since the oxygen in such stars nearly completely is bound in the very stable CO molecule, the envelopes of C-stars are dominated by a hydrocarbon chemistry producing some kind of soot (For a review of stellar evolution and the physics of C-stars see [13] and [14]).

To investigate the cosmic condensation process, these envelopes of late type stars also methodically are of special interest, because the thermodynamical situation of the condensing gas is subject to well defined boundary conditions [15]: Inside the envelope, near the "photosphere" of the star (which resembles the optical "surface" in a distance of a few 10^{13}cm from

[1] 1 $M_\odot = 2 \cdot 10^{30}$kg, the mass of the sun.

the center), the gas satisfies local thermal equilibrium (LTE) at temperatures above 2000K and particle densities of typically $10^{13}\,cm^{-3}$. Outside the opaque dust envelope at 10^{17}cm the temperatures fall below 100K at particle densities of about $100\,cm^{-3}$ in an extreme non-equilibrium situation, caused by the interstellar UV–radiation. In between, the radiation pressure on the dust grains drives the steady outflow of gas and dust with velocities from a few m/s near the stellar photosphere up to about $20\,km/s$ far outside. The elemental composition, besides minor additives, usually comprises H (90%, approximate number densities), He (9%), C (0.2%), O (0.1%) and N (0.1%), with the dominating reactive species carbon and atomic hydrogen. Thus, the chemistry of the photosphere is dominated by neutral atoms and the most stable molecules CO, N_2 and H_2. Since C–stars approximately radiate like a black body at a temperature in the range between 2000 K and 3000 K, the weak UV-radiation within the opaque envelope causes only a negligible amount of ions. Far outside the composition contains mostly H_2, He, CO, a wide spectrum of hydrogenated graphitic dust grains and, due to the high energy photons of the interstellar radiation field, a broad spectrum of different ions (Fig. 1).

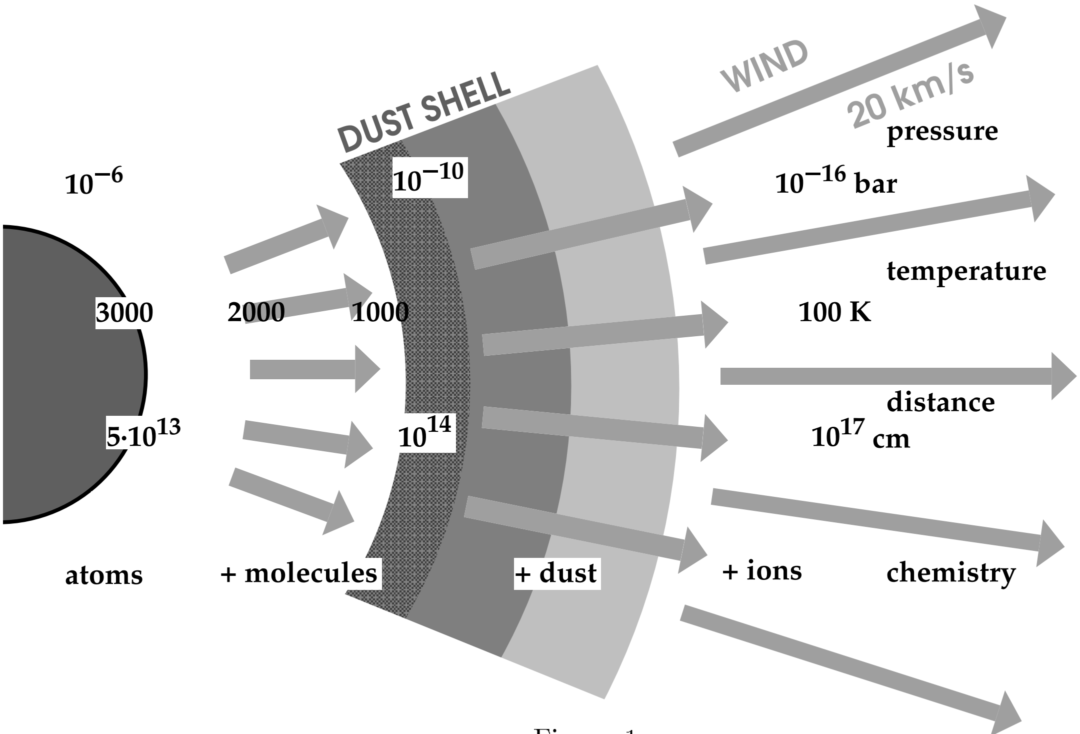

Figure 1:
General schematic structure of a dust forming envelope of a C–star. Like in a flow tube, with increasing distance from the star the temperature drops until condensation occurs. Simultaneously the pressure decreases as well until the chemistry becomes completely frozen. Finally, the chemical composition of the outflow material includes a gas of atoms, complex molecules, and ions with an admixture of dust grains of different sizes.

This situation resembles some kind of gigantic flow-tube experiment with a negative temperature gradient, where the stellar wind guarantees the steady state condition. Initially the gas mainly contains H, H_2 and hydrocarbon species as chemically reactive components of significant abundance, because the CO-component (which is chemically inert in such an environment) blocks nearly all oxygen. The free carbon which is not bound by CO mostly forms acetylene.

Since the outflowing gas initially is free from any condensation nuclei, condensation occurs by molecules, successively taking up acetylene, until the particles have grown to macroscopic sizes. To specify the equilibrium situation of such a condensation process, which our calculations will rely on, we discuss the net growth rates of clusters of different sizes at different temperatures (see Fig. 2). The idea is, to express the behavior of the chemical system, though it is in a metastable subcooled state far away from equilibrium, still by means of equilibrium thermodynamics. For this purpose, "cluster" here denotes a fictitious representative of a class of hydrocarbon molecules *or* small hydrogenated carbon grains ("particles"), defined by their common number of carbon atoms, which shows a "mean" chemical and physical behavior of the class, whereas "molecule" always means a particular structure.

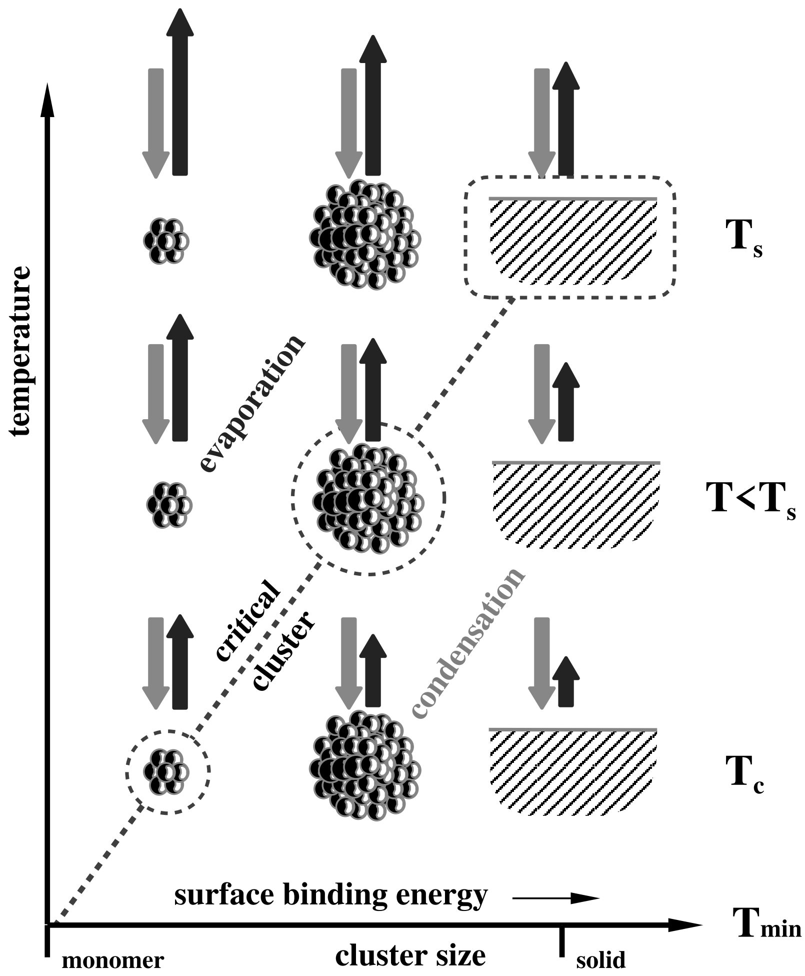

Figure 2:
The critical cluster at different temperatures and a fixed gas pressure in a size-temperature diagram. The very right symbols represent solid surfaces, T_s is the sublimation temperature. Arrows symbolize rates per surface unity: Growth rates (light) predominate for larger clusters (grains), evaporation rates (dark) for smaller ones. The size of metastable equilibrium defines the critical cluster.

The net growth rate of such a cluster is determined by the difference between the rate of growth by reactive collisions with molecules from the gas phase (light arrows) and spontaneous evaporation from the surface of the particle (dark arrows). The growth rates per unit surface area do not depend on the cluster resp. grain sizes, but they are proportional to the mean collision frequency, which varies with temperature as $\sqrt{T}$. Contrariwise, the evaporation rate exponentially depends on T and the total binding energy E_a of surface atoms as $\exp\{-\frac{E_a}{RT}\}$, where R is the universal gas constant. E_a generally decreases with decreasing cluster size: atoms located at curved surfaces are less strongly bound than those at flat surfaces. As a consequence ot this, the evaporation rate increases with decreasing cluster size. For a very small cluster, then, the evaporation rate may well exceed the growth rate even at a temperature far below the sublimation temperature T_s of the bulk condensate, though at the same temperature and gas particle density a big particle with an essential flat surface does grow from the gas phase. As is shown in nucleation theories (for a review of classical nucleation theory see e.g. [16]), a growing particle in such a situation has to overcome a nucleation barrier, below which evaporation dominates, until it enters into the size region of unimpeded particle growth. The size of the cluster representing this barrier (the *critical cluster*) drastically decreases with decreasing temperatures.

Thus, we have the following thermodynamical situation in a dust forming stellar envelope: The gas in the steady radial outflow from the central star has to cool down far below the sublimation temperature T_s. It becomes highly supersaturated with respect to the solid, but relaxation towards chemical equilibrium (CE) at first is hindered by the impossibility to surmount the nucleation barrier. Clusters *smaller* than the critical cluster preform a random walk in the space of cluster sizes, where each growth step is followed with a slightly higher probability by an evaporation step. The particle densities of clusters in this size regime relax to a state where they are very close to the condition of detailed balancing (DB) between growth and destruction steps. Clusters *larger* than the critical cluster, however, undergo nearly exclusively growth reactions: Since within the condensation zone the stellar wind in addition causes constantly falling pressures and temperatures, until the chemistry is completely frozen, the partial pressures of those larger particles remain far below their values where DB is realized. Thus, the nucleation rate equals the growth rate of the critical cluster, the partial pressure of which, in turn, is determined by the DB condition. Effective nucleation occurs, as soon as the critical cluster shows sufficient densities to allow for a growth step into the size regime of pure growth with a significant rate.

This analysis of the physical situation justifies the separation of the chemical problem into two complementary parts, which are divided by the critical cluster size:

1. *Seed formation*: The critical cluster and all smaller clusters are formed in a state of DB, which justifies the application of the law of mass action for calculating the partial pressures in this size regime. The size of the critical cluster, which represents the borderline between the two equilibrium regimes, is a direct result of the calculations: The first reaction step along the pathway from atoms to the solid which is far away from DB, defines the growth rate of the critical cluster. Thus, the identity of the critical cluster likewise marks the borderline of the validity of this CE-analysis in the phase space of molecular sizes. Once the chemical pathway is known (in a particular thermodynamical situation), the clusters can be identified with particular hydrocarbon molecules. Especially the critical cluster itself represents a unique molecular structure which likewise defines the actual *nucleus* of the current nucleation process.

2. *Cluster growth*: Clusters which are larger than the critical cluster, on the other hand, undergo subsequent growth reactions which are controlled by the time scales of the stellar wind. The partial pressures of these intermediates are not mainly determined by their molecular stability, but by the reaction kinetics of their growth. The net outcome of this part of the reaction chain is the formation of *one* macroscopic grain from any single critical cluster which overcomes the nucleation barrier. In this picture, the nucleus, which is identical with the critical cluster, is the largest unity *within* one particular grain, which has retained its identity during the *complete* growth phase.

(Before formation of the critical cluster, an "idendity" of a molecule makes no sense because of many subsequent substitutions.) The size of the final dust grain mainly depends on the mean rate of one typical growth reaction step, besides some influence of the typical geometry and structure of the newly formed solid. Therefore, this part of the chemistry in a dust forming stellar envelope can be modeled with sufficient accuracy within the cluster-picture by a so called "moment method" without knowledge of the details of the chemical pathway. This method is described by Gail and Sedlmayr [17].

As a result of this discussion, it becomes obvious that cosmic condensation processes essentially differ from typical laboratory experiments. During the *cluster growth process*, only the addition reactions of the most abundant reactive carbon bearing species significantly contribute to the cluster growth. Any other type of reactive collisions, because of its by orders of magnitudes lower frequency, are completely negligible. In particular also any agglomeration of larger particles is far below competing with the acetylene addition. Thus, the growth process can be considered as a *polymerization process* with acetylene being the *monomere*, which likewise is the monomere of the corresponding nucleation process in the classical picture.

On the other hand, during *seed formation* many different reactions do contribute to the detailed balancing between the intermediate molecules. Because of the extremely low densities together with the *absolute absence* of any foreign nuclei or surfaces, the gas shows a pronounced metastability with a high supersaturation ratio (10^4 to 10^5) and a distinct nucleation barrier. Nevertheless, a detailed analysis of the chemistry has to complete the application of classical nucleation theory to derive reasonable timescales for the relaxation of the gas towards chemical equilibrium.

In this paper, we support the opinion that carbon dust in C-stars is formed by a nucleation process, resulting in very small aromatic molecules, followed by a progressive and irreversible build up of giant molecules, which gradually become carbon grains by internal structural changes. Unless the current chemical analysis has led to a selfconsistent modeling of the complete dust forming envelope, the only encouragements for this opinion are the *observed* highly effective soot production of the C-stars, the compelling nature of the chemical argumentation and the lack of any alternative idea, which is quantitatively convincing under astrophysical conditions.

3 Methods and scope

One major point of this analysis is the calculation of partial pressures of all relevant hydrocarbons from acetylene up to a size of 26 C-atoms, including important intermediate radicals. The calculations are based on a chemical composition for a typical carbon-rich stellar envelope ($[\mathrm{C}]/([\mathrm{H}]+2[\mathrm{H}_2])=0.0005$), and cover the range from 10^{-6} to 10^{-13} bar and 1200 K to 500 K in the p, T-plane.

Along the chemical pathway to large polyaromatic hydrocarbons, we investigate partial pressures in a metastable, highly supersaturated situation of "hindered condensation". Thus, the commonly used approach of total densities of hydrocarbons above the surface of the solid in our case is not suitable. Instead of this, we have to relate the partial pressures to the "reservoir" of "monomers" of the polymerization, which is the acetylene molecule. For this purpose, and to achieve generality regarding non-equilibrium, we consider a universal formation reaction of PAHs and related molecules from acetylene,

$$j\,\mathrm{C_2H_2} + k\,\mathrm{H} \longrightarrow \mathrm{C}_n\mathrm{H}_m + l\,\mathrm{H_2}\ , \tag{1}$$

with the stoichiometric conditions $n = 2j$ and $m = 2j + k - 2l$ (note that k and l are allowed to be negative). Application of the law of mass action to reaction (1), according to the condition of detailed balancing *below the critical reaction*, leads to an expression for the partial pressure of the molecule under consideration

$$p_{\mathrm{C}_n\mathrm{H}_m} = \frac{p^j_{\mathrm{C_2H_2}} p^k_{\mathrm{H}}}{p^l_{\mathrm{H_2}} p_{\ominus}^{j+k-l-1}} \exp\left\{ \frac{-\Delta_f G^{\ominus}_{\mathrm{C}_n\mathrm{H}_m} - l\Delta_f G^{\ominus}_{\mathrm{H_2}} + j\Delta_f G^{\ominus}_{\mathrm{C_2H_2}} + k\Delta_f G^{\ominus}_{\mathrm{H}}}{RT} \right\} \tag{2}$$

as a function of the partial pressures of C_2H_2, H_2 and atomic hydrogen, the standard state pressure $p_{\ominus} = 1\,\mathrm{bar}$ and the corresponding GIBBS's free-enthalpies. Due to the metastable situation, it is not possible to derive absolute partial pressures which are generally valid irrespective of the particular physical situation, because the derived partial pressures depend on the approach of the equation of mass conservation. Our results presented as relative concentrations with the partial pressure of acetylene as a reference, are *independent* from the approach of mass conservation. To derive from that reliable absolute partial pressures, one has to consider the special non–equilibrium situation, which guarantees that the partial pressures of molecules larger than the critical cluster in any case considerably fall behind their DB values. For this reason, mass conservation may be considered by the relations

$$p_{\mathrm{C_2H_2}} + p_{\mathrm{C_2H_4}} = 1 \quad \text{and} \quad p_{\mathrm{H_2}} = 2000\,, \tag{3}$$

which are good approximations within the whole regime of carbon grain formation between about 1.5 and 3 R_* (stellar radii, see Fig. 1) for species *below* the size of the critical cluster: C_2H_2 (and, for very low temperatures and high pressures, C_2H_4) almost completely contains the reactive carbon, until it may be consumed during grain growth at greater distances from the photosphere, and the concentration of atomic hydrogen in any case falls below that of molecular hydrogen during nucleation. For details see the discussion of section 5.

As far as the GIBBS's free-enthalpies in Eq. (2) are not experimentally known, they have been derived by group-additivity rules [18, 12] or – especially in the case of the heat of formation of the curved large polyaromatic species – by molecular mechanics calculations [19, 20]. Since for a discussion of the chemical pathway a reliable knowledge of the *relative* concentrations is sufficient, the errors in the absolute concentrations, produced by the group-additivity method, can be ignored. Furthermore, because of the numerical uncertainties of polynomial fits of heat capacities, we refrain from calculating explicitly temperature dependent free-enthalpies. As a consequence of the "compensation effect" regarding the temperature dependence of enthalpy and entropy [18], the use of fixed values for the heat of formation and the molecule entropy at 1000 K (which is a typical temperature for the dust forming zone) in our case guarantees more reliable results for the relative concentrations with a maximum error of one order of magnitude in the absolute partial pressures (see next section). On the other hand, the errors of the *temperatures*, where the concentrations reach some critical value, are within about 50 K, which is quite sufficient for our analysis (see [12]).

To finally estimate the nucleation rates from the concentrations of the particular critical clusters, we have to calculate the critical rates from addition reactions of the different critical clusters. Since these reactions are single step kinetical reactions, we use ARRHENIUS's law

$$k_f = A\,T^{\alpha}\,e^{-\frac{E_a}{RT}} \tag{4}$$

in connection with a second order rate equation

$$\dot{n}_i = k_f\,n_j n_l - k_r\,n_i n_k \tag{5}$$

for the formation of species i from species j and l, which is generally valid at the extreme low pressures under consideration.

4 Molecular structures and thermodynamical data

To minimize the effort of calculations it is useful, at first to restrict the number of molecules to be considered by general stability arguments, based on the typical chemical composition of a C-star envelope:

$$\varepsilon(\mathrm{H}) : \varepsilon(\mathrm{C}) : \varepsilon(\mathrm{O}) : \varepsilon(\mathrm{N}) : \; = 1000 : 2 : 1 : 1 \tag{6}$$

The resulting chemistry essentially is determined by the ratio of $\varepsilon(\mathrm{C}) : \varepsilon(\mathrm{O})$, which by definition for all C-stars is larger than unity. The CO-molecule, which according to a stellar situation is the by far most stable molecule, blocks nearly all the oxygen. Since nitrogen mainly forms N_2 with a small amount of CN and HCN, the important molecules have to be hydrocarbons, with an at most small admixture of N, O, Si or S bearing molecules. The lowest limit of number densities of particles which may contribute to an effective nucleation process, can be estimated by the typical number density of grains in such dust envelopes: Every critical cluster which undergoes the critical reaction step becomes *one* macroscopic grain and the critical cluster approximately represents the species with the minimum partial pressure along the chemical pathway. A typical carbon grain contains about $N_{gr} = 10^9$ carbon atoms, which results in a typical partial pressure p_{crit} (relative to acetylene) of the critical cluster of

$$p_{crit} \approx f/N_{gr} \gtrsim 10^{-12} \tag{7}$$

with the degree of condensation $f > 10^{-3}$ in the case of effective nucleation. In our analysis, we omit for this reason molecules which never exceed a partial pressure of $10^{-15}\, p_{\mathrm{C_2H_2}}$ within the investigated range of p and T.

Hydrocarbon molecules show three types of hybridization, which classify the different structures:

- **sp**: sp-orbitals are linear and solely allow the formation of chain molecules of polyacetylenic or allenic type. An estimate of the equilibrium constant of the growth reaction
$$\mathrm{C}_m\mathrm{H}_{2i} + \mathrm{C_2H_2} \rightleftharpoons \mathrm{C}_{m+2}\mathrm{H}_{2i} + \mathrm{H_2} \tag{8}$$
of a chain of length m by group additivity shows that the concentration of chains drops drastically with increasing length: for polyacetylenes by about $2 \cdot 10^{-4} \cdot 10^{200\,K/T}$ per acetylene addition, for allenic chains by $0.1 \cdot 10^{-4\,500\,K/T}$ (with a greater uncertainty caused by resonance energy). Thus, it is obvious that only short polyacetylenes up to about $C_{10}H_2$ or cumulenes up to C_4H_4 may play an important role.

- **sp^2**: This type is represented by polyaromatic hydrocarbons (PAHs), graphite and fullerenes, which are stable at the considered temperatures and pressures, as far as they are very large or completely conjugated, which in most cases rules out molecules with odd numbers of carbon atoms. For radicals see below.

- **sp^3**: The stability of diamond like bonding can be discussed regarding the smallest sp^3 molecule with H/C$\leq$1, which is the cubic cubane C_8H_8. An estimation of the partial pressure yields[2]

$$\log\left(\frac{p_{C_8H_8}}{p_{C_2H_2}}\right) \approx -35.9 + 3\,\log\,p_g[\mathrm{bar}] + \frac{15\,600\,K}{T} \quad , \tag{9}$$

which at pressures under consideration is far below -15 down to about 325 K.

To investigate the influence of a substitution of foreign atoms within the aromatic ring, we estimate the relative concentrations of furan (C_4H_4O), pyrrole (C_4H_5N) and pyridine (C_5H_5N) to benzene. Again we convert the values from Pedley et al. [21] ($\Delta_f H^{\circ}$ = -34.9(furan), 108.3(pyrrole), 140.4(pyridine) kJ/mol) for 1 000 K, using the group data from Benson [18], and we finally derive

$$\begin{aligned}
\log\left(\frac{p(\mathrm{furan})}{p(\mathrm{benzene})}\right) &\approx \quad 4.1 - \frac{17\,600\,K}{T} \quad \lessapprox -13.5 \\
\log\left(\frac{p(\mathrm{pyrrole})}{p(\mathrm{benzene})}\right) &\approx \quad 4.2 - \frac{13\,100\,K}{T} \quad \lessapprox -8.5 \\
\log\left(\frac{p(\mathrm{pyridine})}{p(\mathrm{benzene})}\right) &\approx \quad 1.2 - \frac{9\,200\,K}{T} \quad \lessapprox -8.0 \quad .
\end{aligned} \tag{10}$$

Heteroaromatic molecules thus also play a minor role.

sp^2 hydrocarbon molecules exist as 2-dimensional PAHs or as fullerenes. In a hydrogen-free situation, cage molecules are the most stable structures at sizes exceeding about 30 C-atoms. There exist two theories of formation: either they are formed by completely dehydrogenated PAH structures [22] or by large monocyclic rings [23]. In the first case, the intermediate radicals in a C-star chemistry will be partially saturated by the hydrogen, which blocks further closure to a cage molecule [24]. In the second case, a significant number of very large monocyclic rings has to be formed as intermediates. Since those rings are only slightly more stable than the corresponding linear radical chain with (for 30 C-atoms) a partial pressure of about 10^{-60}, they practically also do not exist in those environments. Independent of the different formation theories of fullerenes, we therefore conclude that the formation of fullerenes in C-star envelopes is kinetically forbidden.

To estimate the influence of the low pressure on the degree of saturation of the remaining hydrocarbon molecules, we proceed from Eq. 2 in the case of chemical equilibrium with $k = 0$. The Gibb's free-energy is substituted by enthalpy H and entropy S via $\Delta G = \Delta H - T\Delta S$, where the entropy change of the reaction roughly is given by the translational contribution S^{tr}:

$$\Delta S = S_{C_nH_m} - \frac{n}{2} S_{C_2H_2} + \frac{n-m}{2} S_{H_2} \approx (1 - \frac{m}{2}) S^{tr} \quad . \tag{11}$$

With Eq. (11) and the substitution $p_{C_2H_2}/p_{\ominus} \approx \tilde{p}_{tot}\epsilon_C$, where $\tilde{p}_{tot} \approx \tilde{p}_{H_2}$ is the total gas pressure in [bar] and ϵ_C the abundance of free carbon in terms of hydrogen, we derive from Eq. (2)

$$\frac{p_{C_nH_m}}{p_{\ominus}} \approx \exp\left\{\frac{S^{tr}}{R}\right\} \epsilon_C^{n/2} \left[\tilde{p}_{tot} \exp\left\{-\frac{S^{tr}}{R}\right\}\right]^{\frac{m}{2}} \exp\left\{-\frac{\Delta H}{RT}\right\} \quad . \tag{12}$$

[2] From Pedley et al. [21] we find $\Delta_f H^{\circ}$(cubane) = 622.1 kJ/mol, Cp's and S are derived by group additivity from Benson [18] (including 6×ring–correction(cyclobutane)), resulting in $\Delta_f H$ = 590.3 kJ/mol and S = 562.9 J/K mol at 1000 K.

For fixed molecule size n, the right hand side of Eq. (12) besides the first two constant factors shows two variable terms. The last factor exponentially depends on the *energy* of the molecule and favors flat polyaromatic (hexagonal) structures with maximum resonance and minimum strain energy. The last but one factor depends on the *entropy* and varies with the total gas pressure like a half-integer power of the number of hydrogen atoms in the molecule. Since this factor predominates for extreme low gas pressures, there is a competition between energy and entropy:

- *minimum energy*: Only polyaromatic, hexagonal flat structures.
- *maximum entropy*: As few hydrogen atoms as possible, carbon preferably with cubic or closed structures.

$\longrightarrow$ *Compromise*: Polyaromatic hexagonal structures with a reduced periphery, curved by isolated pentagons.

Whereas for laboratory conditions the balance between C-H bonds and different types of C-C bonds already produces a maximum of molecular stability at a particular value of m for each class of hydrocarbons with constant n [12], the competition between energy and entropy at low pressures shifts this equilibrium slightly towards even lower m-values. In stellar envelopes, this maximum only is reached, when further removement of hydrogen atoms does not result in (1) additional binding orbitals in the carbon framework, (2) an increase of resonance energy *and* (3) causes a large increase of strain energy. Consequently, in the shells of carbon stars we expect a predominance of highly unsaturated hydrocarbons compared to laboratory. Furthermore, larger PAHs should be curved by pentagons inserted within the carbon framework (see also [2]).

In spite of the significantly lower stability of hydrocarbon radicals, Eq. (12) shows that the energy cost of the unpaired electron may be compensated by the additional translational entropy of the free hydrogen atom. Thus, some radicals may compete in abundance with their related closed shell structures (at higher temperatures, where a high ΔS is favored), or the temperature is too low to provide the reaction activation energies, thus favoring the rates of reactions with radicals. For these reasons, this analysis explicitly includes a considerable number of radicals up to 3-vinylene-acenaphthylene ($C_{14}H_9$). According to the group additivity approach, the addition of a side chain radical to larger molecules or a hydrogen abstraction can be calculated by analogy to the smaller molecules. Such molecules as far as necessary for the analysis of reaction rates also have been included in our present analysis.

The special case of propargyl (C_3H_3), which is a radical with an even total number of atoms, cannot be discussed by general arguments. Its influence can be estimated by the relation of the rates of the two competing hypothetical growth reactions

$$\begin{aligned} \text{I: } C_3H_3 + C_3H_3 &\longrightarrow C_6H_6^* \\ \text{II: } C_4H_4 + C_2H_2 &\longrightarrow C_6H_6^* \quad . \end{aligned}$$

Growth of the propargyl radical to an intermediate of sufficient stability is likely only for the addition reaction (I) with itself. This reaction occurs without activation energy and results in an highly activated complex, marked by "$*$". The same activated complex can be produced by reaction (II) which in any case occurs for a sufficiently activated fraction of educts. Considering the activation energy, the rates roughly relate as

$$Q = \frac{\mathrm{rate(I)}}{\mathrm{rate(II)}} = \frac{p^2_{\mathrm{C_3H_3}}}{p_{\mathrm{C_2H_2}} p_{\mathrm{C_4H_4}} \exp\{-E_a/RT\}} \quad . \tag{13}$$

The relation of the partial pressures can be derived by Eq. (2). The heats of formation and entropy of propargyl is calculated by the group additivity approach by propargyl $\approx$ allene + vinyl − ethene with the data from Benson [18], resulting in $\Delta_f H_{1000\,\mathrm{K}} = 420.72\,\mathrm{kJ/mol}$ and $S_{1000\,\mathrm{K}} = 356.28\,\mathrm{J/K\,mol}$. The activation energy of acetylene to vinylidene is known to be $E_a = 159\,\mathrm{kJ/mol}$ [25]. With this data, the formation of hexadienyne by propargyl falls behind the formation from butenyne and acetylene by $Q = 4 \cdot 10^{-6}$ at 1 300 K resp. $Q = 8 \cdot 10^{-18}$ at 500 K, which is negligible within the scope of our analysis.

As a result of this discussion, the following types of species have to be investigated in detail:

1. even numbered unbranched chains of alkenyne type up to $C_{10}H_2$,
2. fused polyaromatic hydrocarbons (PAHs) including hexagonal and isolated pentagonal structures and short side chains from benzene up to the (unknown) transition to some kind of graphitic or amorphous carbon grain[3], and
3. univalent radicals which are formed by hydrogen abstraction from the preceding molecules.

According to the existence of a maximum of stability for a sequence of hydrocarbons C_nH_m with constant n at a particular m, for each of the two types of hybridization a small range of m-values has been considered. For polyacetylenes, the stability maximum occurs at $m = 2$, thus we investigate chains from $m = 0$ to $m = 4$, and for PAHs the stability maximum ranges from $m = 6$ for benzene to $m = 12$ for acecoronylene ($n = 26$). The structures which have been selected by these rules and investigated throughout this paper are shown in Fig. 3.

To calculate the $\Delta_f G^{\ominus}$ in Eq. (2) at 1 000 K, we need the enthalpies, entropies and heat capacities of 30 groups, including some new groups for radicals and pentagonal structures. The complete set of data is shown in table 1.

For some of the data new estimates or corrections have to be made. Especially, the treatment of resonance energy in our case follows the model GA2(RE) of Herndon et al. [19], because the method of Benson, who included the resonance energy into the C_B-type groups, is not sufficient for large PAHs, which generally do not have all π-electrons delocalized. We calculate the resonance energy by the expression $E_{res} = -123.05\ \ln(\text{Kekulé-counts})$, whereas the model GA3(RE) is not appropriate in our case, because it refers to bonds and not to groups [19]. Nevertheless, for most of our molecules, especially the curved ones and those with pentagons, we prefer the heats of formation resulting from molecular mechanics calculations ([19] and [20]) instead of the group values to correctly consider the strain energy. For the calculation of the entropy, symmetry correction by $R \ln \sigma$ (σ= symmetry number) has been included in the molecular data, whereas the degeneracy factor has been neglected, because it is marginal compared to the uncertainties of the enthalpies of the radicals.

With the group data for 298 K we calculate the heats of formation $\Delta_f H$ of the investigated molecules at 1000 K by using a second order polynomial determined by the change of the heat

[3] Here, the largest molecule considered is benzo[c]picene $C_{26}H_{16}$

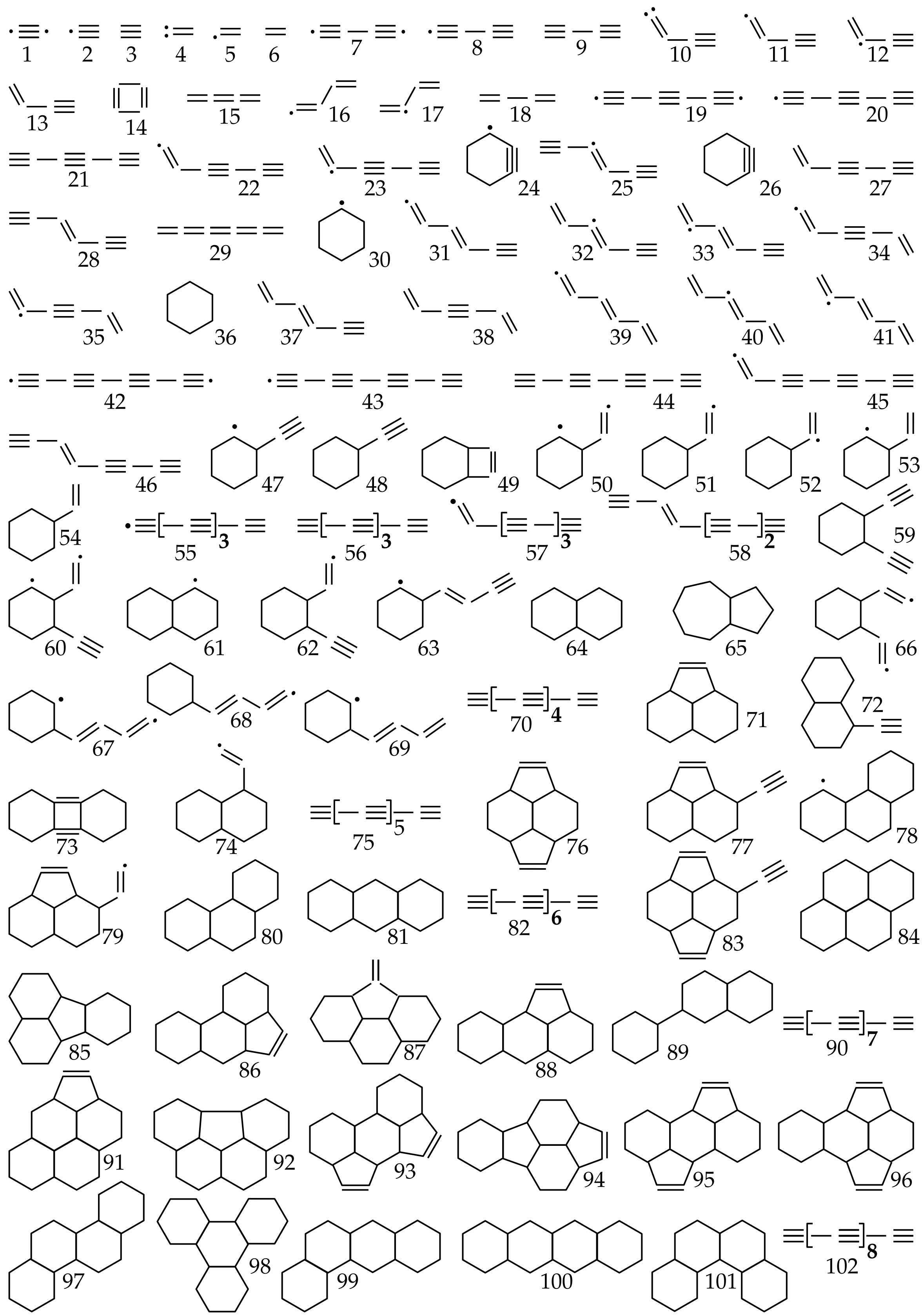

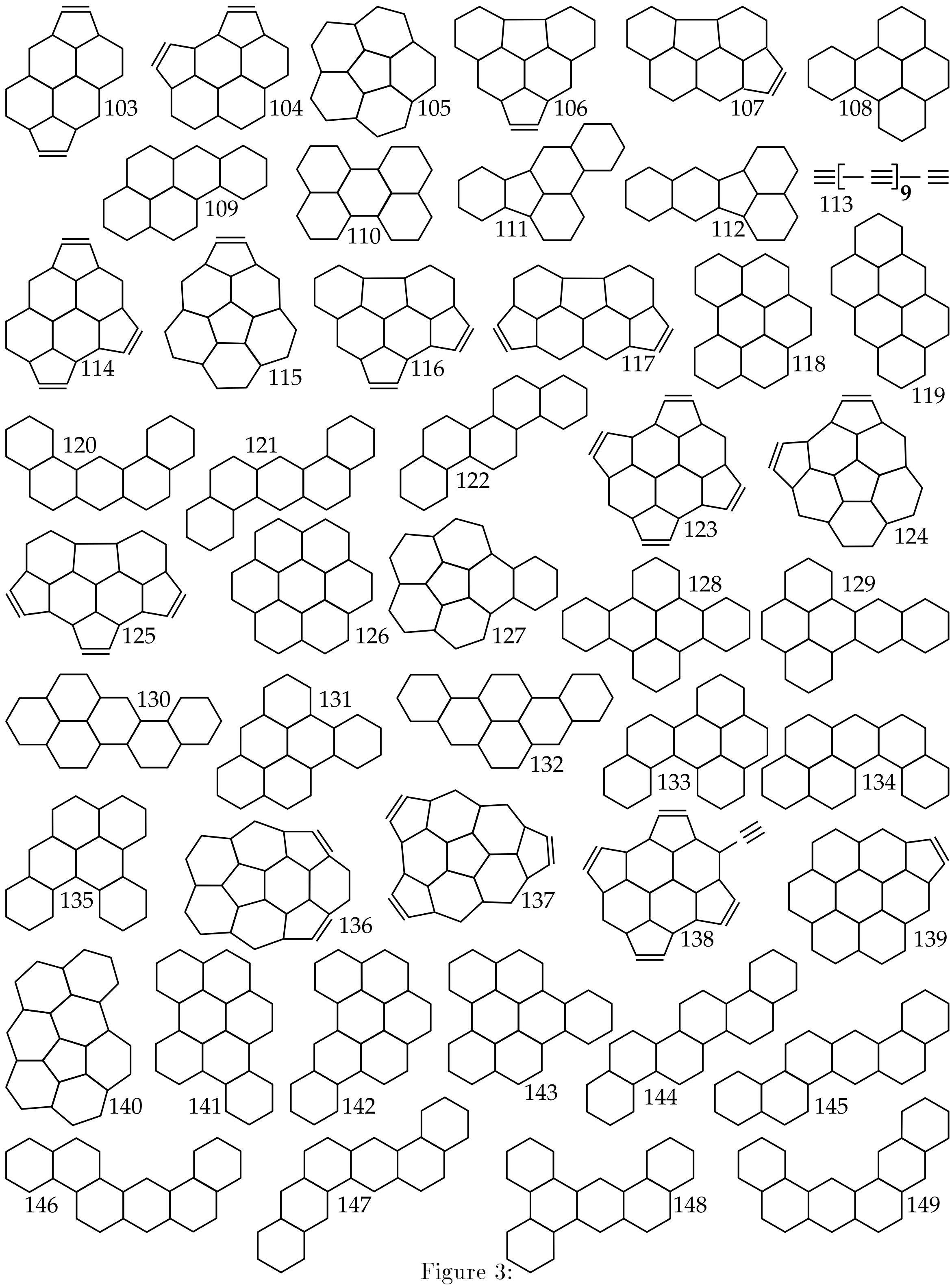

Figure 3:
Structures of hydrocarbon molecules investigated.

group	ref.	$\Delta_f H^{\circ}_{298}$	S°_{298}	$C_p^{\circ}(T)$			
				300 K	500 K	1 000 K	1 500 K
[$\cdot$C$_t$]	1	422.0	104.1	15.2	15.3	17.3	18.2
[:C$_d$]	2	360.0	106.6	12.8	14.6	18.8	21.4
[$\cdot$C$_d$-(H)]	3	254.1	120.2	18.8	23.7	31.4	36.6
[$\cdot$C$_d$-(C$_d$)]	4	257.9	33.5	14.2	19.7	23.0	23.4
[$\cdot$C$_d$-(C$_t$)]	5	257.9	33.5	14.2	19.7	23.0	23.4
[C$_d$-(H)$_2$]		26.2	115.5	21.5	31.2	47.0	55.0
[C$_d$-(C$_d$)(H)]		28.4	26.7	18.6	28.2	38.1	42.2
[C$_d$-(C$_t$)(H)]		28.4	33.6	18.6	28.2	38.1	42.2
[C$_t$-(H)]		112.7	103.3	22.1	27.4	33.8	37.5
[C$_t$-(C$_d$)]		118.0	26.9	11.0	19.0	23.1	23.9
[C$_t$-(C$_t$)]		107.1	24.6	14.8	18.4	21.9	23.3
[C$_a$]	6	143.2	25.1	16.3	19.7	23.0	23.9
[$\cdot$C$_d$-(C$_B$)]	7	257.9	33.5	14.2	19.7	23.0	23.4
[C$_{tB}$]	8	233.5	47.6	10.0	13.1	17.3	19.1
[C$_d$-(C$_B$)(H)]		28.4	26.7	18.6	28.2	38.1	42.2
[C$_t$-(C$_B$)]		103.2	26.9	11.0	19.0	23.1	23.9
[C$_B$-(H)]	9	28.3	48.2	13.8	23.1	35.1	40.3
[C$_B$-(C$_d$)]	10	38.3	-32.6	14.0	16.9	23.2	25.8
[C$_B$-(C$_B$)]	10	35.2	-36.1	12.9	19.2	25.1	26.8
[C$_B$-(C$_t$)]	10	38.3	-46.6	14.0	16.9	23.2	25.8
[$\cdot$C$_B$]	10	272.6	43.2	10.8	14.8	19.3	20.8
[C$_{BF}$-(C$_{BF}$)(C$_B$)$_2$]	9	28.0	-20.9	12.6	17.5	23.7	25.8
[C$_{BF}$-(C$_{BF}$)$_2$(C$_B$)]	9	35.2	-20.9	12.6	17.5	23.7	25.8
[C$_{BF}$-(C$_{BF}$)$_3$]	9	27.7	7.6	8.4	16.3	22.4	23.7
[P$_{S2}$]	11	196.8	101.2	63.7	98.0	137.9	153.6
[P$_{S1,S2}$]	12	198.0	-76.0	58.8	86.3	117.2	126.9
[P$_{S3}$-(C)]	13	327.3	21.6	55.8	90.7	127.3	139.3
[P$_{S3}$-(C$_d$)]	14	225.9	-90.4	57.9	84.3	118.1	130.1
[P$_{S4}$]	15	262.8	-19.0	50.4	83.9	114.6	122.7
[P$_{int}$]	16	393.9	38.0	42.0	81.5	112.0	118.5

Table 1:
Group values for unsaturated hydrocarbons. The units are kJ, mol, K, reference state is graphite and molecular hydrogen at 1 bar and 298 K. We generally follow the group notation of Benson [18], but the [C$_B$-]-groups do *not* include resonance energy. The structures corresponding to the 6 newly defined pentagon-groups are shown in Fig. 4. Values without comments are from Stein and Fahr [12], detailed comments to references see text.

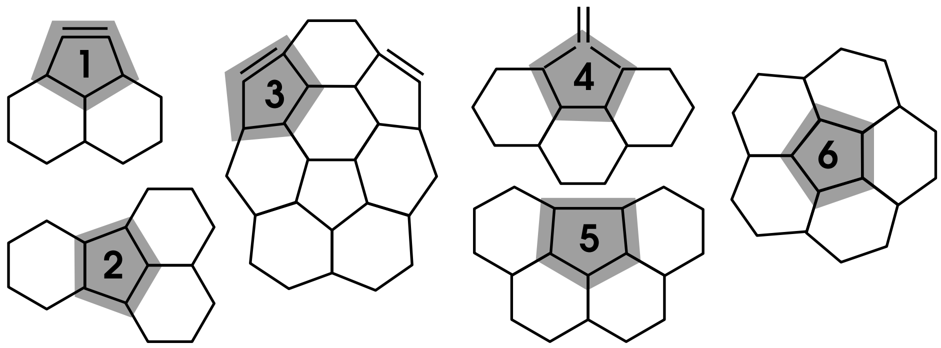

Figure 4:
Structures of the six new defined groups including pentagons: (1)[P_{S2}], (2)[$P_{S1,S2}$], (3)[P_{S3}-(C)], (4)[P_{S3}-(C_d)], (5)[P_{S4}], (6)[P_{int}]. The group values comprise all five carbon atoms. The subscripts denote the structure of the hexagonal framework, where the pentagon is taken up, and follow the nomenclature introduced by Herndon et al. [19]: $S1$ is any site of benzene, Sn ($n > 1$) means a concave edge with $n - 1$ C_{BF}-groups, *int* denotes pentagons completely enclosed into the hexagonal framework.

capacities during formation reaction at 300, 500 and 1000 K. Similarly, the heat capacities of the species itself lead to another second order polynomial to derive the entropy S at 1000 K. These values allow to calculate the temperature dependent GIBBS's free-enthalpies within the interesting temperature interval from 500 to 1200 K with sufficient accuracy. An upper limit of the errors of this calculation method has been estimated by alternatively calculating the partial pressures of the most stable isomers (stabilomers) from the heats of formation and entropies at 298 K via $\Delta G(T) \approx \Delta_f H^{\ominus} - T\,S^{\ominus}$, which leads to values which never differ from the former ones by more than one order of magnitude. This corresponds to an absolute error of the GIBBS's free-enthalpies of less than 5 kJ/mol which is quite negligible compared to the error of the group values.

The results of these calculations for the molecules from Fig. 3 are given in Table 2 with some following comments regarding the references of that data which is not calculated by strict application of the group additivity methods. In the table, those isomers which have the same group values, including the heats of formation, are represented by only one structure. Isomers with the same group values for entropies and heat capacities, but slightly differing heats of formation from molecular mechanics calculations, are also lumped together to one class of molecules, but listed in the table with all corresponding isomers. In the following calculations, any class with n_{iso} isomers is represented by one member only. Consequently, for this representatives the partial pressures have to be corrected with a factor according to the number n_{iso} of isomers and the rotational symmetry numbers σ_i of each isomer.

Since the group values still include a correction for symmetry, the correction factor is given by $ICF = \sigma_1 \sum 1/\sigma_i$, where the index $i = 1$ denotes the representing isomer. For the determination of σ, which in some cases depends on the degree of excitation of the molecules, we assume internal rotations and migrations of radical sites to occur immediately, whereas migrations of H atoms are considered in any case to lead to distinguishable isomers. ghostview

Table 2:
Molecular data of unbranched hydrocarbons and PAHs. The structures of Fig. 3 are listed according to their number. "*" denotes names analogue to IUPAC rules which are not standard. The number of isomers of molecular classes with the same group data are given by n_{iso}. ICF denotes the isomer correction factor (see text). The units are kJ/mol and J/K mol.

nr.	IUPAC name	formula	n_{iso}	ICF	$\Delta_f H(T)$ 298 K	$\Delta_f H(T)$ 1000 K	$S(T)$ 298 K	$S(T)$ 1000 K
1	ethynylene	C2	1	1	837.7	840.1	199.4	245.0
2	ethynyl	C2H	1	1	534.7	532.3	207.4	260.6
3	acetylene	C2H2	1	1	225.4	222.3	200.8	269.3
4	vinylidene	C2H2	1	1	386.2	378.2	216.3	275.4
5	vinyl	C2H3	1	1	280.3	269.1	235.7	306.4
6	ethylene	C2H4	1	1	52.4	37.9	219.5	300.7
7	butadiynylene	C4	1	1	970.7	970.7	228.3	306.5
8	butadiynyl	C4H	1	1	748.9	750.3	256.6	355.4
9	butadiyne	C4H2	1	1	439.6	440.2	250.0	364.2
10	butadiynylidene	C4H2	2	2	619.1	619.3	270.4	382.3
11	1-buten-3-ynyl	C4H3	1	1	513.2	510.2	284.0	407.5
12	1-methylidene-2-propynyl	C4H3	1	1	514.8	511.5	279.2	401.7
13	butenyne	C4H4	1	1	285.3	279.0	273.5	407.6
14	cyclobutadiene	C4H4	1	1	314.0	311.4	213.5	353.0
15	butatriene	C4H4	1	1	338.8	329.7	281.2	411.2
16	1,3-butadienyl	C4H5	1	1	337.1	325.7	289.1	431.2
17	1-methylidene-allyl	C4H5	1	1	338.7	326.9	291.2	432.4
18	1,3-butadiene	C4H6	1	1	109.2	94.4	278.6	431.3
19	hexatriynylene	C6	1	1	1272.4	1278.3	300.8	430.0
20	hexatriynyl	C6H	1	1	963.1	968.2	305.8	450.3
21	hexatriyne	C6H2	1	1	653.8	658.1	299.2	459.0
22	l-hexenediynyl	C6H3	1	1	727.4	728.2	333.2	502.3
23	1-methylidene-2,4-pentynyl	C6H3	1	1	729.0	729.4	328.4	496.6
24	2-benzyne-1-yl	C6H3	2	2	739.4	725.5	277.2	419.1
25	1-ethynyl-1-buten-3-ynyl	C6H3	1	1	747.7	752.6	327.5	502.8
26	benzyne	C6H4	1	1	495.1	478.3	282.2	435.5
27	1-hexenediyne	C6H4	1	1	499.5	496.9	328.5	508.2
28	3-hexenediyne	C6H4	1	1	518.2	520.1	321.8	508.6
29	hexapentene	C6H4	1	1	625.2	621.6	325.6	504.3
30	phenyl	C6H5	1	1	329.0	312.0	278.4	447.2
31	1,3-hexadienynyl	C6H5	1	1	570.0	566.8	337.4	532.3
32 33	1-vinyl-1-buten-3-ynyl 1-methylidene-2-penten-4-ynyl }	C6H5	3	3	571.6	568.0	339.5	533.5
34	1,5-hexadienynyl	C6H5	1	1	573.1	567.0	356.7	545.7
35	1-methylidene-4-penten-2-ynyl	C6H5	1	1	574.7	568.2	351.9	540.0
36	benzene	C6H6	1	1	84.7	64.9	268.5	448.7
37	1,3-hexadienyne	C6H6	1	1	342.1	335.6	332.7	538.2
38	1,5-hexadienyne	C6H6	1	1	345.2	335.7	346.2	545.8
39	1,3,5-hexatrienyl	C6H7	1	1	393.9	382.3	342.5	556.1
40 41	1-vinyl-1,3-butadienyl 1-methylidene-2,4-pentadienyl }	C6H7	2	2	395.5	383.5	344.6	557.3
42	octatetraynylene	C8	1	1	1486.6	1496.2	350.0	524.8
43	octatetraynyl	C8H	1	1	1177.3	1186.1	355.0	545.1
44	octatetrayne	C8H2	1	1	868.0	876.0	348.4	553.8
45	1-octentriynyl	C8H3	2	2	941.6	946.1	382.4	597.2
46	3-octentriynyl	C8H4	3	3	710.6	714.7	372.2	603.4
47	ethynylphenyl	C8H5	3	2.5	554.9	543.6	319.6	537.7
48	ethynylbenzene	C8H6	1	1	310.6	296.4	318.8	548.3
49	cyclobutenobenzene	C8H6	1	1	371.0	360.1	175.2	410.1
50	vinylenephenyl	C8H6	6	6	621.5	605.0	350.3	576.5

nr.	IUPAC name	formula	n_{iso}	ICF	$\Delta_f H(T)$		$S(T)$	
					298 K	1000 K	298 K	1000 K
51	styryl	C8H7	2	2	377.2	357.9	355.3	592.9
52	vinylidenebenzene							
53	vinylphenyl	C8H7	3	2.5	393.6	373.8	345.6	582.4
54	styrene	C8H8	1	1	149.3	126.7	344.8	593.0
55	decapentynyl	C10H	1	1	1391.5	1404.0	404.2	640.0
56	decapentyne	C10H2	1	1	1082.2	1094.0	397.6	648.7
57	1-decen-tetraynyl	C10H3	2	2	1155.8	1164.0	431.6	692.0
58	3-decen-tetraynyl	C10H4	5	4.5	924.8	932.6	421.4	698.3
59	1,2-diethynylbenzene	C10H6	1	1	536.5	528.0	354.2	633.0
60	vinylene-2-ethynylphenyl	C10H6	12	10	856.0	847.4	393.8	671.8
61	naphthyl	C10H7	2	2	398.1	378.1	338.8	612.1
62	1-ethynyl-2-vinylenebenzene	C10H7	2	2	518.8	506.6	321.0	609.3
63	1-buten-3-ynylphenyl	C10H7	6	5	626.5	614.9	393.9	683.4
64	naphthalene	C10H8	1	1	150.3	127.4	332.3	617.0
65	azulene	C10H8	1	1	320.7	297.8	338.0	622.7
66	1,2-divinylenebenzene	C10H8	1	1	669.7	650.9	415.6	710.6
67	1,3-butadienylenephenyl	C10H8	12	10	678.3	661.6	403.7	701.4
68	1,3-butadienylenebenzene	C10H9	4	4	434.0	414.5	408.7	717.7
69	1,3-butadienylphenyl	C10H9	6	6	450.4	430.4	404.8	713.0
70	dodecahexyne	C12H2	1	1	1296.4	1312.0	446.8	743.6
71	acenaphthylene	C12H8	1	1	259.7	239.5	363.7	691.4
72	ethynylnaphthalene	C12H8	2	2	396.9	379.7	379.2	713.2
73	biphenylene	C12H8	1	1	419.3	404.9	229.7	566.5
74	vinylidenenaphthalene	C12H9	4	4	442.8	420.5	409.9	752.0
75	tetradecaheptyne	C14H2	1	1	1510.6	1530.0	496.0	838.5
76	pyracyclene	C14H8	1	1	451.8	434.3	383.7	754.3
77	ethynylacenaphthylene	C14H8	1	1	504.0	489.5	404.9	781.9
78	phenanthrenyl	C14H9	1	1	456.1	433.1	393.4	771.2
79	3-vinylideneacenaphthylene	C14H9	2	2	547.2	527.5	435.6	820.7
80	phenanthrene	C14H10	1	1	207.9	182.0	392.6	781.9
81	anthracene	C14H10	1	1	230.9	205.0	386.9	776.1
82	hexadecaoctyne	C16H2	1	1	1724.8	1748.0	545.2	933.4
83	3-ethynylpyracyclene	C16H8	1	1	700.9	689.1	430.6	850.6
84	pyrene	C16H10	1	1	225.7	202.1	402.1	832.5
85	fluoranthene	C16H10	1	1	289.0	266.1	379.3	811.4
86	acephenanthrylene	C16H10	1	1	318.0	294.8	424.1	856.3
87	fulveno[1,2,3,4-*def*]phenanthrene	C16H10	1	1	336.9	314.2	363.1	796.3
88	aceanthrylene	C16H10	1	1	352.7	329.5	424.1	856.3
89	2-phenylnaphthalene	C16H12	2	2	246.1	216.0	464.4	917.5
90	octadecanonyne	C18H2	1	1	1939.0	1966.0	594.4	1028.3
91	cyclopent[*cd*]pyrene	C18H10	1	1	368.5	347.6	439.3	912.7
92	indeno[7,1-*cd*]phenanthrene	C18H10	1	1	374.5	353.8	394.5	867.8
93	cyclopent[*hi*]acephenanthrylene	C18H10	1	1	441.4	420.9	444.0	919.2
94	cyclopent[*cd*]fluoranthene	C18H10	1	1	464.8	444.6	405.0	880.1
95	cyclopent[*hi*]aceanthrylene	C18H10	1	1	473.2	452.7	444.0	919.2
96	cyclopent[*fg*]aceanthrylene	C18H10	1	1	538.8	518.3	444.0	919.2
97	chrysene	C18H12	4	1.83	276.3	247.4	447.2	941.0
98	triphenylene							
99	benz[*a*]anthracene							
100	naphthacene							
101	benzo[*c*]phenanthrene	C18H12	2	2	291.2	261.6	481.5	973.6
102	eicosadecyne	C20H2	1	1	2153.2	2184.0	643.6	1123.2
103	dipentacyclo[*cd*, *jk*]pyrene	C20H10	1	1	514.9	496.6	459.2	975.6
104	dipentacyclo[*cd*, *mn*]pyrene	C20H10	1	1	515.7	497.4	459.2	975.6
105	corannulene	C20H10	1	1	522.5	504.0	396.4	910.8

nr.	IUPAC name	formula	isomers	ICF	$\Delta_f H(T)$		$S(T)$	
					298 K	1000 K	298 K	1000 K
106	inden[7,1,2,3-*lmno*]acephenanthrylene	C20H10	1	1	573.2	555.1	426.0	942.3
107	inden[7,3,2,1-*amno*]acephenanthrylene	C20H10	1	1	582.1	564.0	420.2	936.5
108	benzo[*e*]pyrene	C20H12	1	1	297.5	270.9	462.4	997.4
109	benzo[*def*]chrysene	C20H12	1	1	310.0	283.3	468.2	1003.1
110	perylene	C20H12	1	1	328.3	301.6	468.2	1003.1
111	benzo[*b*]fluoranthene	C20H12	2	2	343.1	317.1	439.7	976.3
112	benzo[*k*]fluoranthene	C20H12	2	3	354.1	328.1	433.9	970.5
113	docosaundecyne	C22H2	1	1	2367.4	2402.0	692.8	1218.1
114	tricyclopenta[*cd*, *fg*, *jk*]pyrene	C22H10	1	1	686.5	644.8	475.5	993.7
115	acecorannylene*	C22H10	1	1	712.4	655.5	498.1	988.9
116	cyclopent[*hi*]inden[7,1,2,3-*lmno*]- -acephenanthrylene	C22H10	1	1	774.3	759.0	451.7	1011.0
117	cyclopent[*cd*]indeno[1,7,6,5-*lmno*]- -fluoranthene	C22H10	1	1	775.8	760.4	445.9	1005.9
118	benzo[*ghi*]perylene	C22H12	1	1	317.0	292.6	477.6	1053.8
119	dibenzo[*def*, *mno*]chrysene	C22H12	1	1	359.2	334.8	477.6	1053.8
120	dibenz[*a*, *h*]anthracene							
121	dibenz[*a*, *j*]anthracene	C22H14	3	3	339.5	307.7	486.9	1085.3
122	picene							
123	tetracyclopenta[*cd*, *fg*, *jk*, *mn*]pyrene	C24H10	1	1	881.2	868.2	504.9	1107.3
124	dicyclopenta[*bc*, *ef*]corannulene	C24H10	2	2	893.3	880.2	461.1	1061.6
125	diindeno[1, 7, 6 − *def*, 6, 7, 1 − *hij*]- -pyracyclene	C24H10	1	1	953.7	941.0	471.6	1073.9
126	coronene	C24H12	1	1	327.1	304.9	477.9	1095.3
127	benzo[a]corannulene	C24H12	1	1	567.9	546.4	464.3	1083.3
128	dibenzo[*fg*, *op*]naphthacene							
129	dibenzo[*de*, *qr*]naphthacene							
130	benzo[*pqr*]picene	C24H14	5	13	377.6	348.0	511.3	1150.8
131	naphtho[4,3,2,1-*def*]chrysene							
132	benzo[*rst*]pentaphene							
133	naphtho[1, 8, 7 − *ghi*]chrysene							
134	dibenzo[*c*, *mno*]chrysene	C24H14	3	3	389.5	359.2	551.3	1189.1
135	dibenzo[*def*, *p*]chrysene							
136	dicyclopenta[*bc*, *ef*]benzo[d]corannulene	C26H10	1	1	1064.3	1053.9	398.3	1039.7
137	tricyclopenta[*bc*, *ef*, *kl*]corannulene	C26H10	2	2	1079.8	1069.3	486.8	1130.3
138	1-ethynyl-tetracyclopenta- -[*cd*, *fg*, *jk*, *mn*]pyrene	C26H10	1	1	1130.5	1123.2	551.8	1203.5
139	acecoronylene*	C26H12	1	1	469.9	450.4	518.5	1178.9
140	naphtho[2, 1, 8 − *bcd*]corannulene	C26H12	1	1	618.4	599.1	485.3	1145.5
141	dibenzo[*b*, *pqr*]perylene							
142	dibenzo[*b*, *ghi*]perylene	C26H14	3	2.5	393.2	365.8	538.0	1218.7
143	naphtho[4, 3, 2, 1 − *ghi*]perylene							
144	benzo[*c*]picene							
145	naphtho[1, 2 − *b*]chrysene							
146	naphtho[2, 1 − *b*]chrysene	C26H16	6	11	409.5	374.6	556.4	1259.2
147	naphtho[1, 2 − *b*]triphenylene							
148	benzo[*c*]pentaphene							
149	benzo[*a*]pentaphene							

5 The equilibrium stabilities

From the data of Table 2, using Equation (2), we derive equilibrium concentrations with respect to acetylene of the relevant hydrocarbons up to a size of 26 carbon atoms. As far as we restrict to an analysis based on detailed balancing, only the most stable isomer of any size n and m is of interest. Figure 5 shows the structures of those "stabilomers" for a temperature of 800 K. The identity of the stabilomer does not depend on pressure and changes only in few cases as a function of temperature. This behavior is due to the influence of the entropy, which increases proportional with the temperature.

With an exception of five species, our results agree with the stabilomers found at higher temperatures by Stein and Fahr [12]. These deviations are a consequence of our new data:

— We found phenanthrene (80) to be 50 times more abundant than anthracene (81), based on new experimental heats of formation from Pedley et al. [21]. For higher temperatures, the predominance of phenanthrene even increases. The group data used by Stein and Fahr [12] is not suitable to consider the much lower resonance energy of the -acene type PAHs.

— benzo[c]phenanthrene (101), in spite of its significant strain energy by H–H repulsion (the structure is *not* flat [19]), is about 6 times more abundant than chrysene (97), which is a consequence of its higher entropy. Thus, at high temperatures its predominance even increases. Below about 430 K, chrysene becomes the stabilomer.

— With our data, *p*-dipentacyclopyrene (103) is 10% more abundant than *o*-dipentacyclopyrene (104). Group additivity does not distinguish the relative positions of the cyclopenta–groups. Nevertheless, this difference is irrelevant in our context.

— The partial pressure of dibenzo[def, p]chrysene (135), which Stein and Fahr found to be the $C_{24}H_{14}$ stabilomer [12], is exceeded by naphtho[$1, 8, 7 - ghi$]chrysene (133) at all temperatures, because the former one is less stabilized by resonance energy. The difference of the partial pressures at 800 K is about a factor 6. On the other hand, for the same reasons than benzo[c]phenanthrene (101), naphtho[$1, 8, 7 - ghi$]chrysene also 3.5 times predominates the dibenzo[fg, op]naphthacene (128–133) group at 800 K, which overcomes at temperatures below 480 K.

— The high temperature stabilomer 1-ethynyl-tetracyclopenta-[cd, fg, jk, mn]pyrene (138) is superseded by tricyclopenta[bc, ef, kl]corannulene (137) at temperatures below 790 K. At 600 K the latter one predominates by a factor of 11.

The slight difference between the 1-methylidene-allyl radical (17), which according to our data is the high temperature stabilomer, and the 1,3-butadienyl radical (16) is within the errors of the group data and without relevance for our analysis.

The equilibrium concentrations of the stabilomers (resp. the class of isomers represented by the stabilomer) have been calculated in the range from 1 200 K to 500 K and total particle densities of the gas of $n_g = 10^6$ to $10^{13}\mathrm{cm}^{-3}$. The following tables present a selection of results, where the first five tables, **A** to **E**, show a sequence of successively dropping temperatures, and the last three tables, **F** to **H**, demonstrate the pressure dependence (Table 3). The relative concentrations shown in the tables, regarding its physical meaning in a stellar envelope, have to be cautiously interpreted, since the interpretation essentially depends on the validity of our two major assumptions, which are detailed balancing for the calculated partial pressures and the predominance of acetylene during nucleation:

— On the left side of the single dashed line (|, Table B*ff*) which is defined by the critical cluster, irrespective of the supersaturated non-equilibrium situation, detailed balancing holds. In this case, the calculated relative concentrations well represent the physical situation during the condensation process with high accuracy.

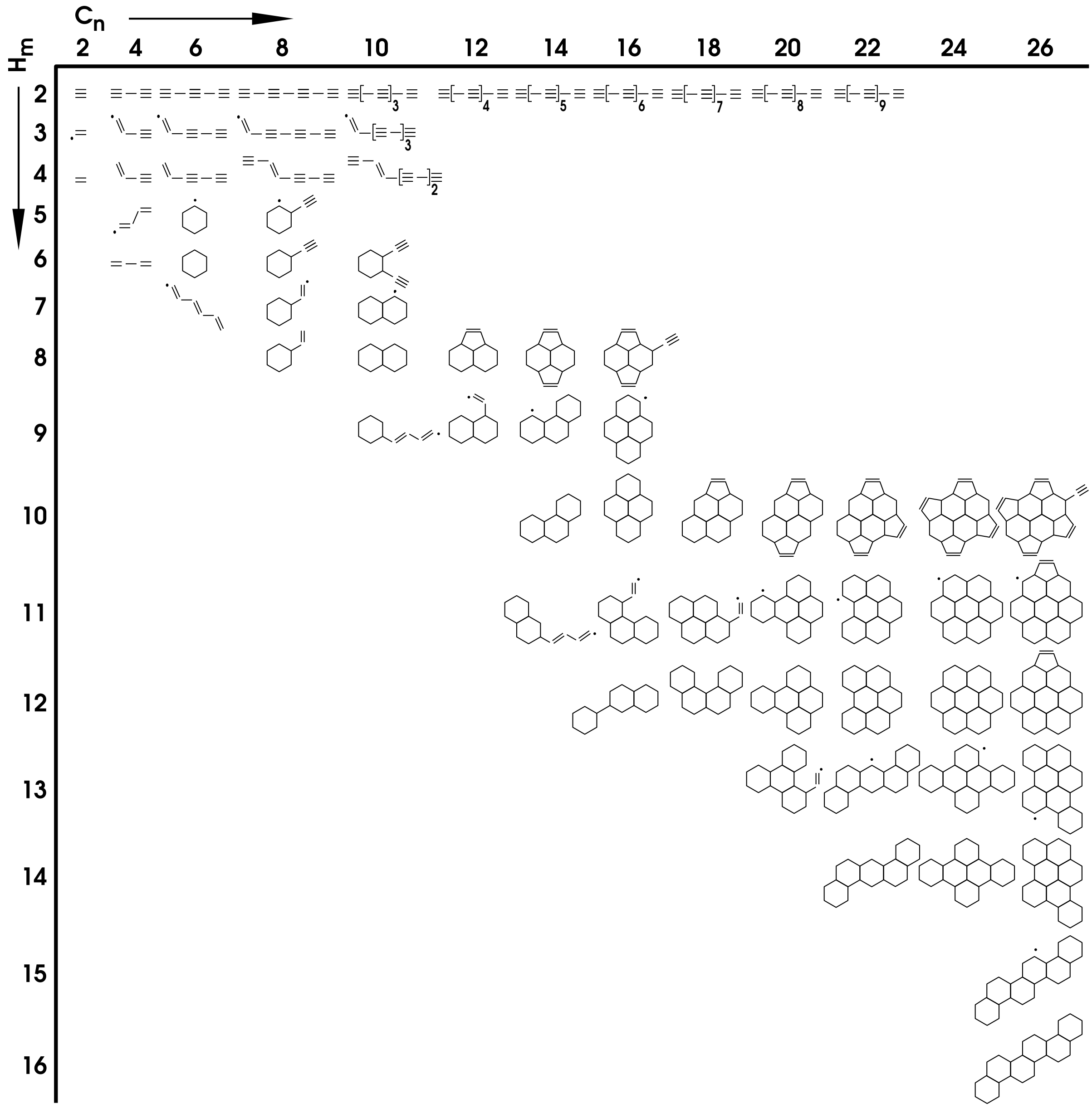

Figure 5: Hydrocarbon stabilomers at $T = 800\,\mathrm{K}$, dependent on the number n of C atoms (ordinate) and the number m of H atoms (abscissa).

— On the right side of the single dashed line, the concentrations of the hydrocarbons are rather controlled by reaction kinetics than by equilibrium stabilities. The numbers may *indicate* the branching ratios of the main reactions, but the actual concentrations more or less will fall behind the equilibrium values.

— As we have outlined in section 3, in the metastable supersaturated gas of a dust forming stellar envelope, the calculation of absolute partial pressures usually only makes sense within a time dependent non equilibrium model. Here, we relate the partial pressures resulting from Eq. (2) to the partial pressure of acetylene, which is frozen until effective grain growth causes its significant consumption. Since on the left side of the double dashed line (||, tables Df and Gf) acetylene (at low temperature and high pressure together with ethylene) is the most abundant C-bearing species, the absolute concentration of acetylene is known from the condition of Eq. (3) and, thus, also the absolute concentrations of the hydrocarbons. This situation is valid during the complete nucleation process, because model calculations show that the consumption of acetylene remains marginal until grain formation stops and effective grain growth begins.

— On the right side of the double dashed line, which is defined by the first molecule exceeding the partial pressure of acetylene, the condition of Eq. 3 is grossly violated. Without a detailed analysis of the reaction kinetics, the equilibrium concentrations have no relevance for the situation in a stellar envelope.

Within every column of the tables, the dominating state of saturation of the carbon cluster of a fixed size n is indicated by bold faced numbers. The growth of an individual carbon cluster (predominantly) occurs via these intermediates, which define a kind of grid along the chemical pathway to large PAHs. Within the range of pressures and temperatures investigated, we distinguished eight of these "zero-order pathways", each being represented by one of the Tables 3, and three subtypes. The corresponding sequences of stabilomers (given by the numbers from Table 2), together with the capital of the corresponding table, are shown in the following list:

I : (**A**) 3 – 9 – 21 – 44 – 56 – 70 – 75 – 82 – 90 – 102 – 113 ⋯

II : (**F**) 3 – 9 – 21 – 44 – 56 – 70 – 75 – 84 – 91 – 103 – **118** – 126 – 139

III : (**B**) 3 – 9 – 21 – 44 – 56 – 71 – 76 – 84 – 91 – **103** – 118 – 126 – 139

IV : (**C**) 3 – 9 – 21 – 44 – 64 – 71 – **76** – 84 – 91 – 103 – 118 – 126 – 139

IVa : 3 – 9 – 36 – 44 – 64 – 71 – **76** – 84 – 91 – 103 – 118 – 126 – 139

V : (**G**) 3 – 9 – 36 – 48 – 64 – 71 – **76** – 84 – 91 – 103 – 118 – 126 – 139

VI : (**D**) 3 – 9 – 36 – **48** – 64 – 71 – 80 – 84 – 91 – 103 – 118 – 126 – 139

VII : (**E**) 3 – **9** – 36 – 48 – 64 – 71 – 80 – 84 – 91 – 108 – 118 – 126 – 139

VIIa: 6 – **9** – 36 – 48 – 64 – 71 – 80 – 84 – 91 – 108 – 118 – 126 – 139

VIIb: 6 – **9** – 36 – 54 – 64 – 71 – 80 – 84 – 91 – 108 – 118 – 126 – 139

VIII : (**H**) **6** – 18 – 36 – 54 – 64 – 71 – 80 – 84 – 91 – 108 – 118 – 126 – 139

A $\log\,(p_{\mathrm{C}_n\mathrm{H}_m}/p_{\mathrm{C}_2\mathrm{H}_2})$ $T = 1200\,\mathrm{K}$ $n_g = 10^{10}\,\mathrm{cm}^{-3}$

$n =$	2	4	6	8	10	12	14	16	18	20	22	24	26
m = 0	-10.7	-12.2	-18.1	-21.7									
1	-5.2	-8.8	-12.3	-15.9	-19.4								
2	**0.0**	**-3.5**	**-7.1**	**-10.6**	**-14.2**	**-17.7**	**-21.3**	**-24.8**	**-28.4**	**-31.9**	**-35.5**		
3	-8.8	-13.1	-16.6	-19.9	-23.4								
4	-7.8	-11.7	-15.0	-18.0	-21.4								
5		-21.2	-18.8	-22.8									
6		-19.9	-16.7	-20.6	-25.3								
7			-33.4	-29.4	-28.3								
8				-28.4	-26.1	-26.1	-30.3	-35.4					
9					-41.5	-39.0	-38.1	-35.0					
10							-35.4	-32.6	-33.8	-36.0	-40.5	-43.3	-48.4
11							-50.1	-48.3	-45.5	-44.9	-42.2	-40.4	-40.3
12								-46.0	-44.0	-42.5	-39.5	-36.9	-37.9
13										-57.9	-57.4	-54.5	-49.8
14											-55.5	-52.1	-48.5
15													-67.1
16													-65.3

B $\log\,(p_{\mathrm{C}_n\mathrm{H}_m}/p_{\mathrm{C}_2\mathrm{H}_2})$ $T = 1000\,\mathrm{K}$ $n_g = 10^{10}\,\mathrm{cm}^{-3}$

$n =$	2	4	6	8	10	12	14	16	18	20	22	24	26
m = 0	-16.0	-16.7	-23.4	-26.9									
1	-7.9	-11.4	-14.9	-18.4	-21.9								
2	**0.0**	**-3.5**	**-7.0**	**-10.5**	**-14.0**	-17.5	-21.0	-24.5	-28.0	-31.5	-35.0		
3	-9.3	-13.7	-17.2	-20.4	-23.9								
4	-6.3	-10.4	-13.6	-16.6	-19.9								
5		-20.3	-15.9	-19.9									
6		-17.0	-11.6	-15.6	-20.4								
7			-31.1	-25.0	-22.1								
8				-22.0	-17.8	**-16.9**	**-20.8**	-26.2					
9					-35.7	-31.3	-28.6	-24.1					
10							-23.7	**-19.2**	**-19.7**	**-21.3**	-25.2	-28.0	-33.3
11							-41.1	-37.2	-32.7	-30.5	-26.0	-22.4	-21.6
12								-32.7	-29.2	-25.9	**-21.1**	**-16.7**	**-17.0**
13										-43.6	-41.5	-37.0	-30.5
14											-37.4	-32.4	-27.0
15													-47.9
16													-43.9

C	$\log\,(p_{\mathrm{C}_n\mathrm{H}_m}/p_{\mathrm{C}_2\mathrm{H}_2})$						$T\,=\,900\,\mathrm{K}\quad n_g\,=\,10^{10}\,\mathrm{cm}^{-3}$						
$n\,=$	2	4	6	8	10	12	14	16	18	20	22	24	26
$m\,=\,0$	-19.6	-19.7	-26.9	-30.4									
1	-9.7	-13.1	-16.6	-20.1	-23.6								
2	**0.0**	**-3.5**	**-7.0**	**-10.4**	-13.9	-17.4	-20.8	-24.3	-27.8	-31.2	-34.7		
3	-9.6	-14.1	-17.6	-20.7	-24.2								
4	-5.2	-9.4	-12.6	-15.6	-18.9								
5		-19.7	-13.9	-18.0									
6		-15.1	-8.2	-12.3	-17.1								
7			-29.6	-22.0	-17.9								
8				-17.7	**-12.2**	**-10.6**	**-14.4**	-20.0					
9					-31.8	-26.2	-22.3	-16.6					
10							-15.9	**-10.2**	**-10.3**	**-10.4**	-14.9	-17.7	-23.3
11							-35.0	-29.9	-24.2	-20.9	-15.3	-10.4	-9.2
12								-23.9	-19.4	-14.8	**-8.9**	**-3.2**	**-3.1**
13										-34.2	-30.8	-25.3	-17.6
14											-25.2	-19.2	-12.6
15													-35.2
16													-29.7

D	$\log\,(p_{\mathrm{C}_n\mathrm{H}_m}/p_{\mathrm{C}_2\mathrm{H}_2})$						$T\,=\,800\,\mathrm{K}\quad n_g\,=\,10^{10}\,\mathrm{cm}^{-3}$						
$n\,=$	2	4	6	8	10	12	14	16	18	20	22	24	26
$m\,=\,0$	-24.0	-23.5	-31.3	-34.7									
1	-11.9	-15.3	-18.8	-22.2	-25.7								
2	**0.0**	**-3.4**	-6.9	-10.3	-13.8	-17.2	-20.7	-24.1	-27.6	-31.0	-34.5		
3	-9.9	-14.6	-18.0	-21.2	-24.6								
4	-4.0	-8.3	-11.4	-14.4	-17.7								
5		-18.9	-11.4	-15.5									
6		-12.6	**-4.0**	**-8.1**	-12.9								
7			-27.6	-18.3	-12.8								
8				-12.3	**-5.2**	**-2.8**	-6.5	-12.2					
9					-27.0	-19.7	-14.3	-7.1					
10							**-6.2**	**1.0**	**1.5**	**0.9**	-2.0	-4.8	-10.5
11							-27.4	-20.7	-13.5	-8.7	-1.6	4.8	6.6
12								-12.8	-7.0	-0.9	**6.5**	**13.7**	**14.4**
13										-22.3	-17.3	-10.4	-1.3
14											-10.0	-2.6	5.4
15													-19.0
16													-11.8

E $\log\,(p_{\mathrm{C}_n\mathrm{H}_m}/p_{\mathrm{C}_2\mathrm{H}_2})$ $T\,=\,600\,\mathrm{K}$ $n_g\,=\,10^{10}\,\mathrm{cm}^{-3}$

$n\,=$	2	4	6	8	10	12	14	16	18	20	22	24	26
$m\,=\,0$	-37.3	-34.8	-44.5	-47.8									
1	-18.6	-21.9	-25.3	-28.6	-32.0								
2	**0.0**	**-3.4**	-6.7	-10.1	-13.4	-16.8	-20.1	-23.5	-26.8	-30.2	-33.5		
3	-11.0	-16.1	-19.4	-22.5	-25.8								
4	-0.1	-4.8	-7.9	-10.7	-13.9								
5		-16.5	-3.8	-8.2									
6		-5.3	**8.9**	**4.6**	-0.5								
7			-21.8	-7.0	2.9								
8				3.9	**15.8**	**20.6**	17.6	11.1					
9					-12.2	-0.3	9.7	21.3					
10							**23.2**	**34.8**	**37.0**	38.0	36.7	33.8	28.7
11							-4.5	7.1	18.7	27.8	39.2	50.2	53.7
12								20.6	30.2	**41.0**	**52.7**	**64.5**	**66.9**
13										13.6	23.1	33.9	47.5
14											35.8	47.1	59.6
15													29.5
16													42.1

F $\log\,(p_{\mathrm{C}_n\mathrm{H}_m}/p_{\mathrm{C}_2\mathrm{H}_2})$ $T\,=\,900\,\mathrm{K}$ $n_g\,=\,10^{7}\,\mathrm{cm}^{-3}$

$n\,=$	2	4	6	8	10	12	14	16	18	20	22	24	26
$m\,=\,0$	-16.6	-16.7	-23.9	-27.4									
1	-8.2	-11.6	-15.1	-18.6	-22.1								
2	**0.0**	**-3.5**	**-7.0**	**-10.4**	**-13.9**	**-17.4**	**-20.8**	-24.3	-27.8	-31.2	-34.7		
3	-11.1	-15.6	-19.1	-22.2	-25.7								
4	-8.2	-12.4	-15.6	-18.6	-21.9								
5		-24.2	-18.4	-22.5									
6		-21.1	-14.2	-18.3	-23.1								
7			-37.1	-29.5	-25.4								
8				-26.7	-21.2	-19.6	-23.4	-29.0					
9					-42.3	-36.7	-32.8	-27.1					
10							-27.9	**-22.2**	**-22.3**	**-23.4**	-26.9	-29.7	-35.3
11							-48.5	-43.4	-37.7	-34.4	-28.8	-23.9	-22.7
12								-38.9	-34.4	-29.8	**-23.9**	**-18.2**	**-18.1**
13										-40.7	-47.3	-41.8	-34.1
14											-43.2	-37.2	-30.6
15													-54.7
16													-50.7

G	$\log\,(p_{\mathrm{C}_n\mathrm{H}_m}/p_{\mathrm{C}_2\mathrm{H}_2})$						$T = 900\,\mathrm{K}$ $\quad n_g = 10^{11}\,\mathrm{cm}^{-3}$						
$n =$	2	4	6	8	10	12	14	16	18	20	22	24	26
$m = 0$	-20.6	-20.7	-27.9	-31.4									
1	-10.2	-13.6	-17.1	-20.6	-24.1								
2	**0.0**	**-3.5**	-7.0	-10.4	-13.9	-17.4	-20.8	-24.3	-27.8	-31.2	-34.7		
3	-9.1	-13.6	-17.1	-20.2	-23.7								
4	-4.2	-8.4	-11.6	-14.6	-17.9								
5		-18.2	-12.4	-16.5									
6		-13.1	**-6.2**	**-10.3**	-15.1								
7			-27.1	-19.5	-15.4		|						
8				-14.7	**-9.2**	**-7.6**	**-11.4**|	-17.0					
9					-28.3	-22.7	-18.8|	-13.1			||		
10							-11.9|	**-6.2**	**-6.3**	**-7.4**	-10.9||	-13.7	-19.3
11							-30.5|	-25.4	-19.7	-16.4	-10.5||	-5.9	-4.7
12							|	-18.9	-14.4	-9.8	**-3.9**||	**1.8**	**1.9**
13							|			-29.3	-25.3||	-19.8	-12.1
14											-19.2||	-13.2	-6.6
15											||		-28.7
16													-22.7

H	$\log\,(p_{\mathrm{C}_n\mathrm{H}_m}/p_{\mathrm{C}_2\mathrm{H}_2})$						$T = 600\,\mathrm{K}$ $\quad n_g = 10^{12}\,\mathrm{cm}^{-3}$						
$n =$	2	4	6	8	10	12	14	16	18	20	22	24	26
$m = 0$	-39.3	-36.8| ||	-46.5	-49.8									
1	-19.6	-22.9| ||	-26.3	-29.6	-33.0								
2	0.0	-3.4| ||	-6.7	-10.1	-13.4	-16.8	-20.1	-23.5	-26.8	-30.2	-33.5		
3	-10.0	-15.1| ||	-18.4	-21.5	-24.8								
4	**1.9**	-2.8| ||	-5.9	-8.7	-11.9								
5		-13.5| ||	-0.8	-5.2									
6		**-1.3**| ||	**12.9**	8.6	3.5								
7		| ||	-16.8	-2.0	7.9								
8		| ||		**9.9**	**21.8**	**26.6**	23.6	17.1					
9					-5.2	6.7	16.7	28.3					
10							**31.2**	**42.8**	**45.0**	46.0	44.7	41.8	36.7
11							4.5	16.1	27.7	36.8	48.2	59.2	62.7
12								30.6	40.2	**51.0**	**62.7**	**74.5**	**76.9**
13										24.6	34.1	44.9	58.5
14											47.8	59.1	71.6
15													42.5
16													56.1

Table 3: Relative logarithmic concentrations of the $\mathrm{C}_n\mathrm{H}_m$ hydrocarbon stabilomers of Figure 5 for $n = 2; 4 \ldots 26$ and $m = 0; 1 \ldots 16$, based on chemical equilibrium. Bold faced: predominant molecule for fixed n. Dashed lines: Borderlines for detailed balancing (|) and the mass conservation assumption (||) in a dynamic stellar envelope (see text).

Since these sequences of stabilomers are only based on equilibrium stabilities, it has to be stressed that they in general do not represent the actual chemical pathway, which has to be found by comparison of reaction rates. Especially the intermediate reaction steps involving radicals are not yet obtained by this equilibrium calculation. The necessary kinetical analysis, because of the large amount of additional reaction data, will be subject of paper II. Nevertheless, unless detailed balancing holds, these stabilomers in fact also are intermediates of the actual pathway, because the rates of the acetylene addition reaction differ much less from each other than the concentrations of molecules of different degree of hydrogenation.

The limits of the condition of detailed balancing can be found by application of the principles of classical nucleation theory on the "zero-order pathway", as discussed in section 2: The stabilomer with the lowest concentration found on the pathway from acetylene to large PAHs (e.g. coronene, which in any case is a part of the pathway), which is printed in bold faced numbers, defines the "critical cluster". The following growth step of the critical cluster by acetylene addition consequently represents the "critical reaction", which is the bottleneck of the condensation process as well as the rate of formation of dust nuclei, so far effective dust formation occurs. Since the critical reaction simultaneously defines the limit of the condition of detailed balancing (marked by "|"), the analysis in this paper provides the definite pathway (resp. the closed shell intermediates of the chemical pathway) only up to the critical cluster, which fortunately is just sufficient for the modeling of stellar dust shells. The results of the present analysis are reliable as a provisional approximation which allows for a classification of the pathways in the pressure-temperature plane and a rough estimate of the nucleation rates.

The sequences of stabilomers show that one crucial point of the pathway is the transition from a linear chain as most stable cluster structure (in any case a polyacetylene) to a benzenoid structure. The position of this "first ring closure" strongly depends on the thermodynamical conditions. In Table **A**, at 1 200 K and $10^{10}\,\mathrm{cm}^{-3}$, the polyacetylenes remain the most stable structures up to 22 C-atoms (which means *one* ring closure within a cubic-kilometer in 10^8 years: benzenoid structures practically do not exist under those conditions), In Table **B**, at 1 000 K and $10^{10}\,\mathrm{cm}^{-3}$, the ring closure occurs for $n = 12$, and for temperatures below $T = 900\,\mathrm{K}$ the first ring molecule already is benzene itself. The ring closure reactions will be closely investigated in paper II.

Another interesting question is the relative stability of clusters of the same size n, but of different degrees of saturation m. Comparing for example the concentrations of butadiynylene, butadiyne and butenyne, we see that for linear chains high pressures as well as low temperatures favor the more unsaturated species. The same tendency can be seen comparing dicyclopentapyrene (103) and benzo[*e*]pyrene (108), and, in spite of the higher strain energy caused by internal pentagons, also comparing corannulene (105) with benzo[*e*]pyrene, which have the same concentrations at 710 K for $n_g = 10^6\,\mathrm{cm}^{-3}$ and at 1 190 K for $n_g = 10^{13}\,\mathrm{cm}^{-3}$. This behavior is the direct consequence of the increasing influence of the translational entropy of the hydrogen, as discussed in section 3 with Eq. (12). For PAHs, it has a very important impact on the question of the topology of very large clusters. If this tendency continues for larger particles – which is very likely, because the influence of the antagonistic strain energy decreases – the large PAHs should more and more incorporate pentagons, which leads to curved graphitic layers, and finally close to some kind of 3-dimensional spiral structure. This behavior also is supported by the tendency of C–C edge bonds to be slightly shorter than resembling internal bonds, because they are more localized. Although this curved species in laboratory chemistry obviously play a minor role, also high pressure analysis shows that with increasing molecular size a curved topology is more and more favorable compared with the "classical" flat graphitic layer, as already has been pointed out by Keller and Herndon [4, 19].

6 Phase diagram and discussion

In a model of a dust forming stellar envelope, two key problems regarding the chemistry essentially determine the macroscopic behavior of the model:

1. Which is the rate of formation of dust nuclei at a particular distance of the star?
2. Which is the growth rate of dust grains at a particular distance of the star?

The second question we here put aside, because it is beyond the scope of the present paper. Regarding the first question, in the previous sections we have shown that the rate of formation of nuclei equals the growth rate of the critical cluster which in turn is the *critical rate*. (This statement holds, at least, as far as the nucleation process is of sufficient efficiency. Since only models of dust envelopes with significant absorption by dust grains are of interest, this condition is automatically satisfied in such cases.) To find the critical rate (for one particular gas element at each instant), we have to know the actual chemical pathway at the particular pressure and temperature. The lowest rate along the most effective reaction chain then defines the critical rate. Any particular gas element in the stellar wind follows a trajectory of monotonously decreasing pressures and temperatures, until the chemistry is frozen at extremely low pressures. Consequently, the chemical pathway and the critical rate have to be known in the whole regime of the p, T-plane which is relevant for stellar envelopes.

Our results allow for a lowest-order analysis of the distribution of chemical pathways to PAHs in the p, T-plane. The procedure is as follows:

- At every point within the p, T-range under consideration, from a grid of tables of hydrocarbon concentrations we determine the type of the particular chemical pathway according to the zero-order approximation described in the previous section.
- Regions of the same type of chemical pathway are separated by lines and labeled by some key molecules (the smallest aromatic molecule after the first ring closure and some isomers of different degree of saturation).
- For every p and T, within the particular zero-order pathway, the closed shell stabilomer with the lowest concentration is identified. This structure corresponds to the "critical cluster", as defined by classical nucleation theory.
- Regions of similar "critical clusters" are likewise separated and labeled by the corresponding structure.

The results are shown in Figures 6 and 7. In Figure 6, the contour lines of the different zero-order pathways are approximately parallel to the line of the solid-gas phase transition of carbon, which is far outside the right margin of the figure (passing $\log n_g = 10$ at 2 230 K [26]). Additionally shown are two typical trajectories of dust driven stellar winds (bold faced dashed arrows): Every gas element starting from the stellar photosphere follows such a trajectory through the p, T-plane with its chemistry being controlled by the local conditions encountered on its way out of the star. The two trajectories belong to a high density ($10^{-4} \mathrm{M}_\odot \, \mathrm{yr}^{-1}$, solar masses per year) and a low density ($10^{-6} \mathrm{M}_\odot \, \mathrm{yr}^{-1}$) stationary wind model. Thus, in spite of the differences in position and slope that such trajectories of different models may have, any trajectory passes through the same sequence of different chemical pathways. Since the efficiency of the condensation (resp. of the particular critical rate) strongly depends on the

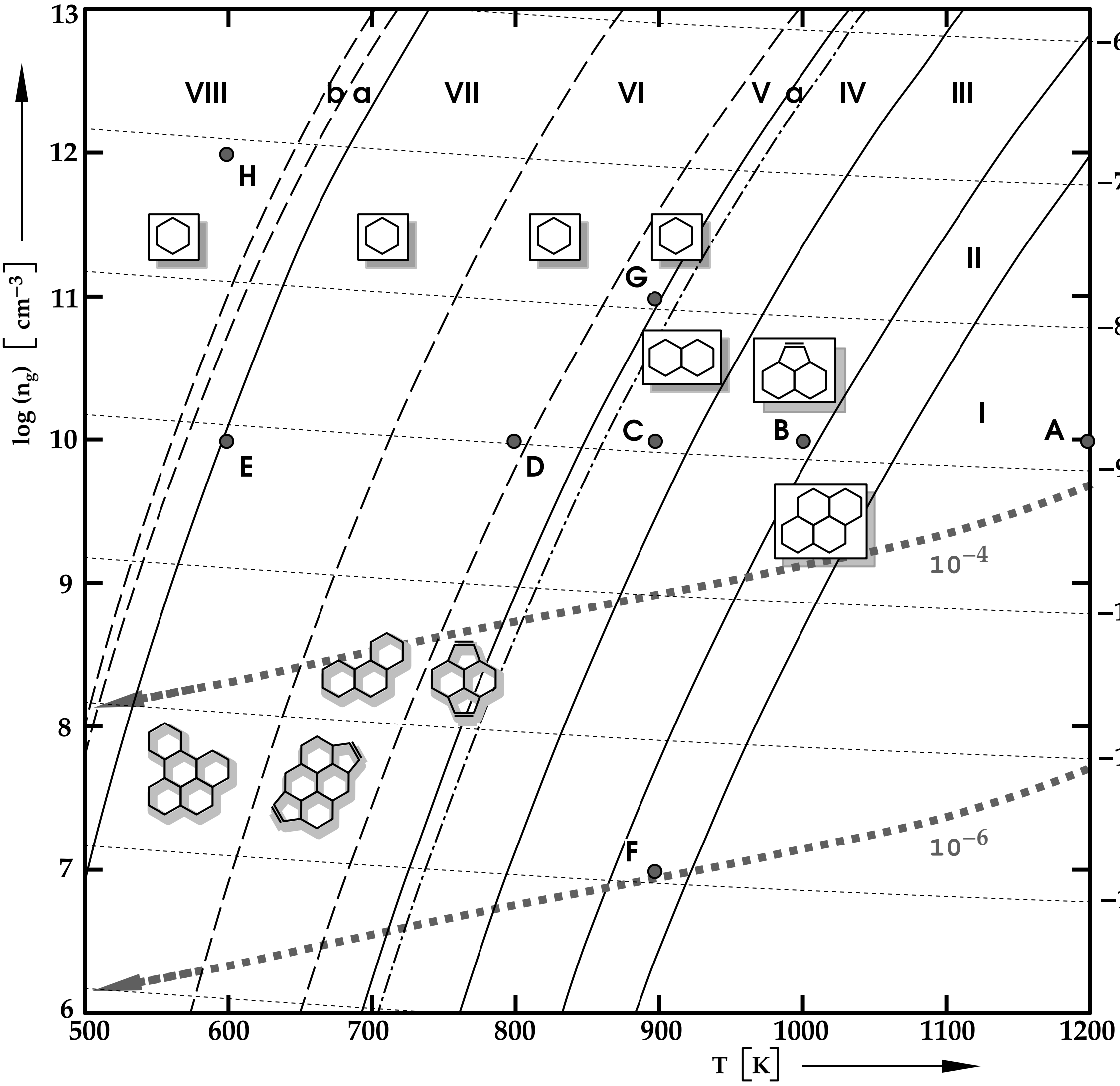

Figure 6: "Zero-order" pathways of carbon condensation in a phase diagram, based on a C-star chemistry. The numbers I to VIII denote the main types of chemical pathways, according to last section. The framed structures show the first aromatic structure which is formed by ring closure from a chain molecule. The dashed–dotted line indicates the first dominance of the ring closure to benzene, whereas within Va after a reactive collision the chemically activated ethynylbenzene may open again to a chain, closing to a naphthyl type radical after an additional growth step. Regarding V, VI and VII, the transition between the corresponding frameless structures defines the borderline between the pathways. Two typical trajectories of dust envelopes of C-stars are shown by grey dotted arrows and marked by the corresponding mass–loss in solar masses per year (see text). The $p-T$–positions corresponding to the concentration tables A to H, each representing one of the main pathways, are marked by grey bullets.

particular position of the gas element within the p, T-plane, we expect the majority of the dust to be within a narrow zone in the p, T-plane which belongs to only *one* single chemical

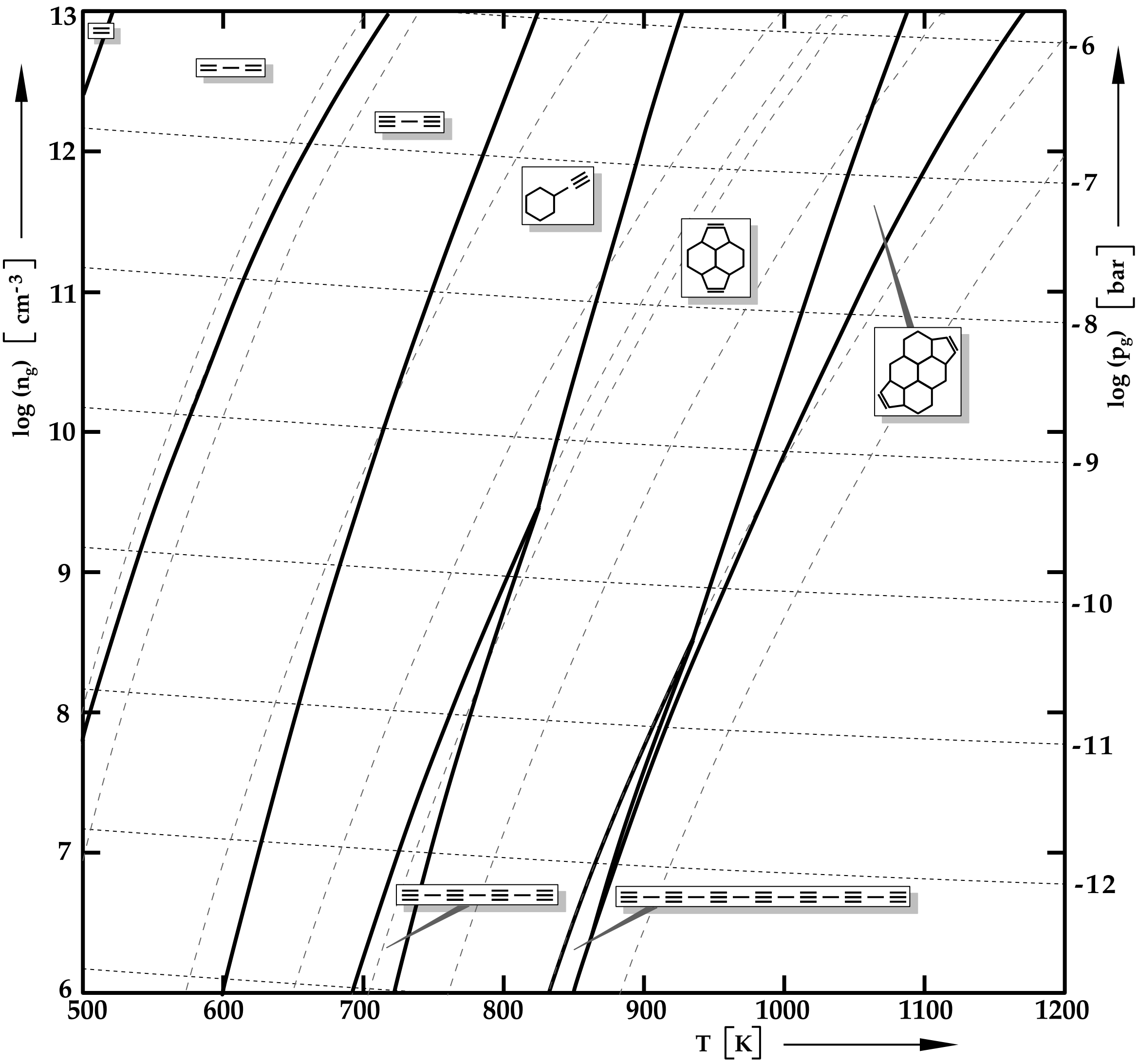

Figure 7: Regimes of the closed shell stabilomers with the lowest equilibrium concentrations within the corresponding chemical pathway from Figure 6, which is approximately the distribution of critical clusters in the p, T-plane. The structures show this "critical clusters" within the areas between the bold faced transition lines. For comparison, the distribution of the pathways from Figure 6 is indicated by thin dashed lines.

pathway. Whether this "effective pathway" is unique for all C-star envelopes has to be investigated by a kinetical analysis and by model calculations.

It should be noted that the wind trajectories shown in Figures 6 and 8 are calculated with a more simplified condensation chemistry and are *not* consistent with our present chemical analysis. They should only be interpreted qualitatively.

Regarding the eight main pathways and the three subtypes there are some interesting details (see Figure 6):

- Since the differences of the free-enthalpies between linear chains and benzenoid structures with equal number n of carbon atoms are very different for each n, the sequence of pathways should include for each size n a reaction step for closure of chains into a ring structure. In contrary to this, our tables show gaps for the structures pyracyclene (76) and ethynylbenzene (48), which never become the product of the first ring closure. The reason is that they are much less stable than the neighbouring smaller benzenoids, which are more readily formed by a first ring closure. As a consequence, there appears a small zone of temperatures (here labeled as IVa), where the triacetylene closes to a benzene radical, but a significant number of the subsequently formed ethynylbenzene molecules may open again to a chain. If this process is kinetically allowed (the chain only is more stable, if the molecule looses hydrogen atoms) and may hinder further growth of the clusters, has to be analyzed by a kinetical approach (see paper II). Such a zone of a less stable second ring molecule also appears for pyracyclene between II and III. Here we have omitted this intermediate pathway in the figure, because the temperature zone only has a width of about 6 K.

- The pathways VIIa/b and VIII differ from the preceding ones by the predominance of the more saturated molecules ethylene (6), styrene (54) and 1,3-butadiene (18) over acetylene (3), ethynylbenzene (48), and butadiyne (9). This tendency again corresponds to the entropy argument discussed in section 4 (Eq. (12)).
- The pathways I and VIII comprise various "pathways" within one class. The subtypes have not been distinguished, because (I) the concentrations are too low for any significant condensation or (VIII) the nucleation barrier has vanished. In the latter case, nucleation completely occurs far away from detailed balancing, and our results are not applicable to the growth process.
- Since the details of the pathway beyond the critical reaction are controlled by reaction kinetics, the classification of pathways by stabilomers which are larger than the critical cluster may be a characteristic of the equilibrium approach without any consequences for the actual pathway of molecular growth. Therefore the separation lines between V and VI, VI and VII, VIIa and VIIb, and VIIb and VIII are of indefinite relevance, which is indicated by dashed lines (— — —). This also holds for the subtypes of pathway VIII, which already have been omitted for other reasons (see last paragraph).

A comparison of Figure 7 with Figure 6 shows that the regions in the p, T-plane which correspond to the same closed shell stabilomer with the lowest concentration along the pathway ("critical cluster") only partly coincide with the regimes of similar pathways. The reason is that the changes of the pathways usually do not befall the identity of the local "critical cluster", and the variations of relative concentrations, causing a change of the identity of the "critical cluster", may occur within one particular chemical pathway. In general we see that there are fewer candidates for the "critical cluster" than there are different pathways: The structures of main interest are butadiyne (9), ethynylbenzene (48) and pyracyclene (76), and with minor importance occasionally 1,3-butadiene (18) and dipentacyclopyrene (103). The small gaps with octatetrayne (44) and tetradecaheptyne (75) correspond to the temporary instability of the second benzenoid structure along of the pathway (see the remarks on the subclasses IVa and the omitted IIa) which are expected to be bridged by kinetical effects. The regimes of benzoperylene (118) or larger structures for the "critical cluster" as well as of ethylene (6) are also of no practical importance (see discussion of the rates).

To get a rough idea of the efficiency of the nucleation process as a function of p and T, Figure 8 shows the results of a lowest-order approximation of the critical rates which determine the formation rate of dust nuclei. Since a detailed kinetical analysis will be subject to paper II, an upper limit of the critical rate has been obtained for the contour plot by the following procedure:

- The addition reaction rate of acetylene with the particular "critical cluster", according to the identification given above[4], has been calculated for any p and T. For the reaction rates, the following Arrhenius'-coefficients have been used (in units cm^{-3}):

$$\begin{array}{rll} \mathrm{C_4H_6} + \mathrm{C_2H_2} & \longrightarrow \mathrm{l\text{-}C_6H_7} + \mathrm{H} & A = 1.7 \cdot 10^{-13} \\ \mathrm{C_4H_2} + \mathrm{C_2H_2} & \longrightarrow \mathrm{c\text{-}C_6H_3} + \mathrm{H} & A = 2.5 \cdot 10^{-14} \\ \mathrm{C_8H_6} + \mathrm{C_2H_2} & \longrightarrow \mathrm{C_{10}H_8} + h\nu & A = 1.7 \cdot 10^{-11} \\ \mathrm{C_{14}H_8} + \mathrm{C_2H_2} & \longrightarrow \mathrm{C_{16}H_{10}} + h\nu & A = 8.3 \cdot 10^{-14} \end{array} \tag{14}$$

  The temperature exponent α in all cases is zero, whereas the activation energy is assumed to be the reaction enthalpy of the formation of vinylidene $(:=)$ from acetylene, which is $E_a = 159\,\mathrm{kJ/mol}$ [25]. The A-values are *maximum possible rates* and have been derived from Frenklach and Feigelson [5]:
  (1) Analogue to $\mathrm{C_4H_4} + \mathrm{C_2H} \rightarrow \mathrm{l\text{-}C_6H_4} + \mathrm{H}$,
  (2) analogue to $\mathrm{C_4H_3} + \mathrm{C_2H_2} \rightarrow \mathrm{c\text{-}C_6H_4} + \mathrm{H}$,
  (3) analogue to $\mathrm{c\text{-}C_6H_5} + \mathrm{C_2H_2} \rightarrow \mathrm{c\text{-}C_8H_7}$,
  (4) analogue to $\mathrm{C_{12}H_9} + \mathrm{C_2H_2} \rightarrow \mathrm{C_{14}H_{11}}$

- The contour lines of similar "critical rates" are continued beyond the borderlines of its region of validity of the corresponding "critical cluster" until they intersect. For lines corresponding to "critical clusters" of different size, the *smaller* rate is relevant (which represents the bottleneck), whereas from intersecting lines of "critical clusters" of different degree of saturation the *larger* rate predominates (which represents the strongest reaction channel). Following the contour lines from intersection to intersection, The continuous, but not differentiable lines give a rough, but simple determination of regimes of significant nucleation rates within the p, T-plane.

The extension of the contour lines beyond the borderlines of the equilibrium regimes of the "critical clusters" until they intersect leads to a shift of the regimes according to the kinetical interpretation of the critical rate. Thus, to allow for a comparison with the equilibrium results, in Figure 8 the borderlines of Figure 7 have been marked by dotted lines as well as the borderlines of Figure 6 within Figure 7.

The results show that the role of ethynylbenzene (48) from the kinetical point of view also seems to be of temporary importance. The efficiency of the nucleation process, as a function of the position of a gas element within the stellar envelope, has to be discussed along of the particular trajectory of the stellar wind, which in general is the result of a selfconsistent model calculation. As an approximation, we consider the relative efficiency along the trajectories in Figure 8, which have been calculated with a more simple treatment of the chemistry. In general, the maximum of efficiency is reached when butadiyne (9) becomes the critical cluster, according to our lowest-order analysis. This occurs at temperatures of about 700 K, if local

[4] The actual critical rate most probably is a reaction of a radical with a closed shell species, with the radical having significantly lower concentrations than a closed shell species, but reacting without activation energy. This two approximation errors of our approach roughly compensate each other.

thermal equilibrium holds, which is a precondition of the present work. Nevertheless, we again have to remind the fact that a reliable determination of condensation temperatures and rates requires a kinetical analysis including radical reactions, which have just the opposite temperature dependence as that of reactions of activated closed shell species considered here (see paper II).

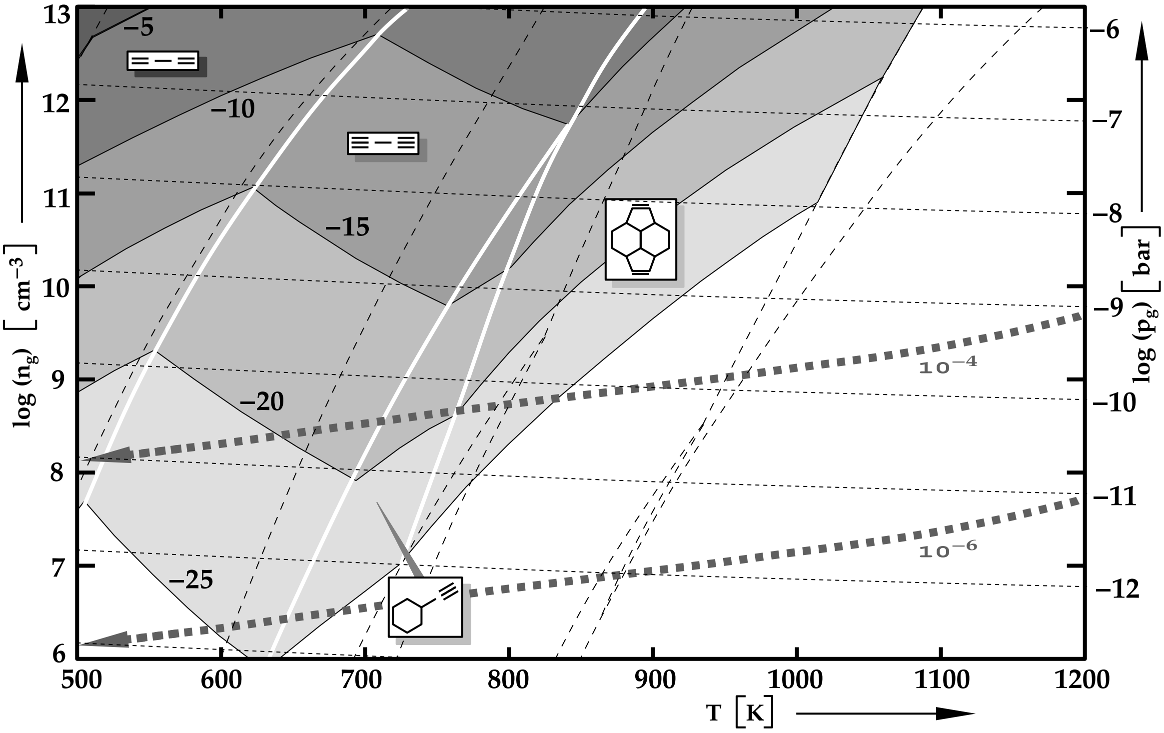

Figure 8: Contour plot of estimated upper limits of the critical rates of carbon condensation in C-star envelopes (see text) in units nuclei/sec·cm^3 in the $p-T$–plane. As a consequence of the kinetical approach, the number of critical clusters in question reduces to four, which are shown within frames. The regimes of the different critical clusters are separated by white lines. Again the two wind trajectories and the boundaries from Figure 7 are shown as dotted arrows resp. lines.

Appendix

In the following we summarize some comments and references regarding the group data of Table 1:

(1) From ethynyl ($\cdot C_2H$) and the [C_t-(H)]-group. $\Delta_f H^{\ominus}$ of ethynyl has been taken from Okabe [27], since the JANAF-value is known to be much too low. $S^{\ominus}$ and C_p's are taken from JANAF-tables [28], which are identical with the values from Benson [18].

(2) From ethylene (C_2H_4) and the difference for abstraction of the two hydrogen atoms of H_2CCO. The values for :CCO are taken from JANAF-tables, since the Benson-value of $\Delta_f H^{\ominus}$ is much too high. Almost the same results can be obtained from vinylidene ($:C_2H_2$).

(3) From vinyl ($H{\cdot}C{=}CH_2$), where the values of $S^{\ominus}$ and C_p's are from Benson [18] and the $\Delta_f H^{\ominus}$ = 280.5 kJ/mol is the mean value of Stull and Westrum [29] resp. Frank and Just [30]. Using in the same way the mean values of 1-butyn-3-ynyl ($\cdot C_4H_3$, $\cdot{=}{-}{\equiv}$) and 1,3-butadienyl

($\cdot C_4H_5$, $\cdot\!=\!-\!=$) from the same authors, we get a 5 kJ/mol lower value for the group. We prefer the more reliable value from vinyl for all three radicals, to obtain consistency with the propargyl-type radicals ($=\!\dot{-}\!\equiv$).
(4) We have used three independent estimates: I) From $CH_3\dot{C}O$ and CH_3CHO [18], with a correction for the substitution of CO by C_2H_2, which has been derived from (vinyl – acetylene) – ($H\dot{C}O$ – H_2CO) (vinyl: s.(3), others: mean value of Benson [18] and JANAF-tables [28])), II) From the group [$\cdot C_d$-(H)], corrected by the substitution of (H) by (C_d) from the groups [C_d-$(H)_2$] and [C_d-(C_d)(H)] and III) from [C_d-(C_d)(H)] by hydrogen abstraction [$\cdot$C-$(C)_2$(H)] – [C-$(C)_2(H)_2$], the last two groups from Benson [18]. The last method yields too small $\Delta_f H^\circ$ (change in hybridization), but reliable C_p's. We chose for $\Delta_f H^\circ$ the mean value of I and II (difference 13 kJ/mol), for S and C_p's the mean value of I to III.
(5) Analogous to the previous group.
(6) Derived from Benson [18]
(7) Analogous to the [$\cdot C_d$-C_d], [$\cdot C_d$-C_t]-groups
(8) From (benzyne – benzene)/2 + [C_B-(H)], $\Delta_f H^\circ$(benzyne) = 494 kJ/mol [31] and $\Delta_f H^\circ$(benzene) = 83.7 kJ/mol [19], S and C_p's from Stein and Fahr [12].
(9) From the GA2(RE)-model of Herndon et al. [19]
(10) Corrected for group data *without* a contribution to resonance energy, according to the GA2(RE)-model of Herndon et al. [19], by adding 1/6 of the resonance energy of benzene which results from the $E_{res} \approx 123\ln$(Kekulé-counts) rule.
(11) From acenaphthylene. (71) From Pedley et al. [21]. This group value exceeds the results of Stein and Fahr [12], which there only denotes the *addition* of acetylene to a naphthalene molecule, by 5 kJ/mol.
(12) From fluoranthene (85, $\Delta_f H^\circ$ = 289.0 kJ/mol, [21]). For S° and C_p's we interpret the carbon atoms to be part of a hexagon, which means neglection of the small difference of pentagonal and hexagonal ring correction.
(13) From dicyclopenta[bc,ef]benzo[d]corannulene (136), $\Delta_f H^\circ$ = 1 064.27 kJ/mol, [20]. For S° and C_p's we take the group values for 2$\cdot$[C_{BF}-$(C_{BF})_3$], 2$\cdot$[C_{BF}-(C_{BF})$(C_B)_2$] and [C_B-(H)].
(14) From fulveno[$1,2,3,4-def$]phenanthrene (87), $\Delta_f H^\circ$ = 336.87 kJ/mol, [20]. For S° and C_p's we take the group values of 2$\cdot$[C_{BF}-$(C_{BF})_2$(C_B)], 2$\cdot$[C_B-(C_d)], [C_d-$(C_B)_2$] and $\frac{3}{5}\cdot$(ring–correction cyclopentene). The [C_d-$(C_B)_2$]-group has been derived from [C_d-$(C)_2$] and [C_d-(C)(C_B)] by analogy [18], the ring correction considers the fact that two C-atoms already has been treated as ring atoms, whereas the three others do not show internal rotations after ring closure.
(15) From indeno[$7,1-cd$]phenanthrene (92), $\Delta_f H^\circ$ = 374.49 kJ/mol, [20]. For S° and C_p's, see (12).
(16) From corannulene (105), $\Delta_f H^\circ$ = 522.49 kJ/mol, [20]. For S° and C_p's we take the [C_{BF}-$(C_{BF})_3$] group values.

From the data of the molecules in Table 2, the entropies and heat capacities of the listed molecules are completely derived by the group data of Table 1, except (1), (2), (6) and (7) (*including* the T = 1 000 K data from JANAF-tables [28]) and (3): In the case of acetylene the JANAF-tables show correct values for 298 K, but a calculation error for all higher temperatures. Thus we take these values from Benson [18]. In the case of (1), (5) and (7), the heats of formation for 298 K and 1 000 K are also derived from JANAF-tables, whereas in all other cases, the values for 1 000 K are calculated. The standard heats of formation are derived from (2) Okabe [27], (3)+(6) Pedley et al. [21], (4) the acetylene value from Pedley et al. [21], corrected by the activation energy from Duran et al. [25]. (14) The value is a mean value of three independent estimation methods: I) From binaphthylene (or dibenzo[b,h]biphenylene) and cyclobuteno[b]naphthalene (both values from SCF-calculations [20]) and subtracting the difference from the latter one: $\Delta_f H^\circ \approx 342\,\mathrm{kJ/mol}$, II) from SCF-values of biphenylene, subtracting the group values according to the GA3(RE)-model of Herndon et al. [19]: $\Delta_f H^\circ \approx 297\,\mathrm{kJ/mol}$ III) from 4 [C_d-(C_d)(H)]-groups, the cyclobutadiene ring correction, derived from the cyclobutene and cyclobutane correction from Benson [18] and the resonance energy calculated by Aihara [32]: $\Delta_f H^\circ \approx 304\,\mathrm{kJ/mol}$, (26) from Dewar et al. [31], (36) from Herndon et al. [19], (49) from the cyclobuteno[b]naphthalene value derived by SCF-calculations by Herndon [20], corrected by the difference of naphthalene and benzene, (64)+(71) from Pedley et al. [21], (77) by correcting the acenaphthylene-value by the SCF-difference for ethynyl addition, (80)+(81) from Pedley et al. [21], (83) by correcting the pyracyclene-value by the SCF-difference for ethynyl addition, (84)+(85)+(97)+(98) from Pedley et al. [21] (138) by correcting the value of tetracyclopenta[cd, fg, jk, mn]pyrene for ethynyl addition, (139) from the value of coronene, corrected by the ace-group of cyclopent[cd]pyrene and (140) from benzo[a]corannulene, corrected by the difference of cyclopent[cd]pyrene and acephenanthrylene. The following values are derived by SCF-calculations of W.C. Herndon with the "ANTHRA" code [20]: (61), (65), (72), (73), (76), (86)-(88), (91)-(96), (99)-(101), (103)-(112), (114)-(137) and (141)-(149). All other values are straight forward results of the group values of Table 1.

Acknowledgements

We are grateful to W.C. Herndon from the University of Texas for kindly calculating geometries and heat capacities of more than 100 polycyclic hydrocarbons with the ANTHRA-code and for helpful discussions.

References

[1] F. Hoyle and N.C. Wickramasinghe. On Graphite Particles as Interstellar Grains. *Mon. Not. R. Astron. Soc.*, 124:417–433, 1962.

[2] R. Keller and E. Sedlmayr. Entstehung von Kohlestaub in Sternhüllen. *Mitt. d. Astron. Ges.*, 60:312, 1983.

[3] A. Léger and J.L. Puget. Identification of the "unidentified" IR emission features of interstellar dust? *Astron. Astrophys.*, 137:L5–L8, 1984.

[4] R. Keller. Polyaromatic hydrocarbons and the condensation of carbon in stellar winds. In A. Léger et al., editor, *Polycyclic Aromatic Hydrocarbons and Astrophysics*, pages 387–397, Dordrecht, 1987. D. Reidel.

[5] M. Frenklach and E.D. Feigelson. Formation of Polycyclic Aromatic Hydrocarbons in Circumstellar Envelopes. *Astrophys. J.*, 341:372–384, 1989.

[6] I. Cherchneff, J.R. Barker, and A.G.G.M. Tielens. Polycyclic aromatic hydrocarbon formation in carbon-rich stellar envelopes. *Astrophys. J.*, 401:269–287, 1992.

[7] M. Rowan Robinson and S. Harris. Radiative transfer in dust clouds IV. Circumstellar dust shells around carbon stars. *Mon. Not. R. Astron. Soc.*, 202:796–811, 1983.

[8] A. Goeres. The Formation of PAHs in C-type Star Environments. In G. Klare, editor, *Reviews in Modern Astronomie Vol.6:Stellar Evolution and Interstellar Matter*, pages 165–177, Hamburg, 1993. Astronomische Gesellschaft.

[9] I. Cherchneff. *Polycyclic Aromatic Hydrocarbon Radiative Properties and Formation in Carbon-rich Stellar Outflows.* PhD thesis, The University of Michigan, Michigan, 1991.

[10] E. Sedlmayr and J.M. Winters. Dust in the shells of cool giants and supergiants. In L. Crivellari et al., editor, *Stellar Atmospheres: Beyond Classical Models*, pages 397–408, Netherlands, 1991. Kluwer Academic Publisher.

[11] A. Goeres, R. Keller, E. Sedlmayr, and H.-P. Gail. Circumstellar Carbon Condensation II: The Chemical Pathway to Polyaromatic Hydrocarbons. submitted to *Polyc. Arom. Comp*, 1996.

[12] S.E. Stein and A. Fahr. High-Temperature Stabilities of Hydrocarbons. *J. Phys. Chem.*, 89:3714–3725, 1985.

[13] I. Iben Jr. Single and binary star evolution. *Astrophys. J. Suppl. Ser.*, 76:55–114, 1991.

[14] H.-P. Gail and E. Sedlmayr. Dust formation in stellar winds. In G.E. Morfill and M. Scholer, editors, *Physical Processes in Interstellar Clouds*, pages 275–303, Dordrecht, 1987. D. Reidel.

[15] E. Sedlmayr. From molecules to grains. In U. G. Jørgensen, editor, *Molecules in the stellar environment*, pages 163–185, Berlin, 1994. Springer–Verlag.

[16] I. Feder, K.C. Russel, I. Lothe, and G.M. Pound. Homogeneous nucleation and growth of droplets in vapours. *Adv. Phys.*, 15:111–178, 1966.

[17] H.-P. Gail and E. Sedlmayr. Dust formation in stellar winds IV. Heteromolecular carbon grain formation and growth. *Astron. Astrophys.*, 206:153–168, 1988.

[18] S.W. Benson. *Thermochemical kinetics.* John Wiley & Sons, New York, 1976.

[19] W.C. Herndon, P.C. Novak, D.A. Connor, and P. Lin. Empirical model calculations for thermodynamical and structural properties of condensed polycyclic aromatic hydrocarbons. *J. Am. Chem. Soc.*, 114:41–47, 1992.

[20] W.C. Herndon. private communication, 1994.

[21] J.B. Pedley, R.D. Naylor, and S.P.Kirby. *Thermochemical Data of Organic Compounds.* Chapman & Hall, London, 1986.

[22] A. Goeres and E. Sedlmayr. On the nucleation mechanism of effective fullerite condensation. *Chem. Phys. Letters*, 184:310–317, 1991.

[23] J.M. Hunter, J.L. Fye, and M.F. Jarrold. Annealing C_{60}^+: Synthesis of Fullerenes and Large Carbon Rings. *Science*, 260:784–786, 1993.

[24] A. Goeres and E. Sedlmayr. Hydrogen-blocking in C_{60}-formation theories. *Fullerene Science & Technology*, 1(4):563–570, 1993.

[25] R.P. Durán, V.T. Amorebieta, and A.J. Colussi. Pyrolysis of Acetylene: A Thermal Source of Vinylidene. *J. Am. Chem. Soc.*, 109:3154–3155, 1987.

[26] A. Goeres. Chemistry and Thermodynamics of the Nucleation in RCrB star shells. Mon. Not. R. Astron. Soc., in press.

[27] H. Okabe. *J. Chem. Phys.*, 62:2782, 1975.

[28] M.W. Chase Jr., C.A. Davies, J.R. Downey Jr., D.J. Frurip, R.A. McDonald, and A.N. Syverud. JANAF Thermochemical Tables. In *J. Phys. Chem. Ref. Dat., Vol.14 Suppl.1.* National Bureau of Standards, 1985.

[29] D.R. Stull, E.F.Jr. Westrum, and G.C. Sinke. *The Chemical Thermodynamics of Organic Compounds.* Wiley, New York, 1969.

[30] P. Frank and Th. Just. *Combust. Flame*, 38:231, 1980.

[31] M.J.S. Dewar, G.P. Ford, and C.H. Reynolds. Ground states of Molecules: 61.Relative Stabilities of *o*, *m*- and *p*-Benzyne. *J. Am. Chem. Soc.*, 105:3162–3167, 1983.

[32] J. Aihara. Aromaticity and Diatropicity. *Pure & Appl.Chem.*, 54(5):1115–1128, 1982.